This is the author's final accepted version.

There may be differences between this version and the published version. You are advised to consult the publisher's version if you wish to cite from it.

Deposited on: 08 May 2017

Triggering Redox Activity in a Thiophene Compound: Radical Stabilization and Coordination Chemistry

Massimiliano Curcio,[a] James R. Pankhurst,[a] Stephen Sproules,[b] Dimitri Mignard,[a] and Jason B. Love*[a]

Abstract: The synthesis, metalation, and redox properties of an acyclic bis(iminothienyl)methene **L⁻** are presented. This π-conjugated anion displays pronounced redox activity, undergoing facile one-electron oxidation to the acyclic, metal-free, neutral radical **L˙** on reaction with FeBr₂. In contrast, reaction of **L⁻** with CuI forms the unique, neutral Cu₂I₂(**L˙**) complex of a ligand-centered radical, whereas reaction with the stronger oxidant AgBF₄ forms the metal-free radical dication **L˙²⁺**.

Since the first reports on dithiolate metal complexes,[1] interest in redox-active ligands has burgeoned due to their relevance to enzymatic processes[2] and access to unusual chemical properties by coupling the redox activity of the ligand to the coordination chemistry of a metal.[3] In these cases, the ligand is no longer a classical "spectator",[4] and a large number of ligands have been shown to exhibit redox activity and stabilize the radical species through an inductive effect or by delocalization in a conjugated π-system.
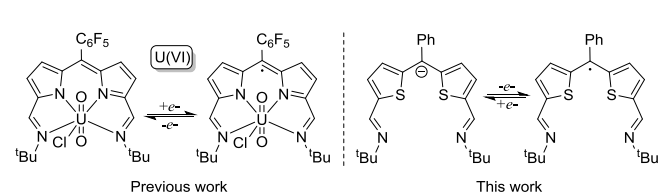

Figure 1. Left: A uranium complex of a redox-active bis(iminopyrrolyl)methene ligand. Right: A redox-active bis(iminothienyl)methene.

Accordingly, we have shown that an N-donor-expanded dipyrrin ligand[5] is redox active and able to mediate sequential electron transfer to a uranyl(VI) center (Figure 1). The initial reduction occurs at the ligand, forming a U(VI) ligand-centered radical prior to reduction of the uranium center, ultimately to U(IV).[6] Ligand-centered oxidation was also seen in Ni complexes of a similar bis(phenolate)dipyrrin ligand, with the one-electron oxidation product characterized as a ligand-centered radical.[7]

In contrast to the nitrogen-containing heterocycles found in dipyrrins, porphyrinoids and sub-porphyrins,[8] studies on the redox activity of sulfur-containing heterocycles such as thiophene are more limited, despite their use in tuning the electronic properties of molecular compounds[9] and polymeric materials.[10] Expanded porphyrinoids featuring five thiophene units undergo single-electron oxidations, from the aromatic mono-anion to an isolable, air-stable neutral radical, and further to an anti-aromatic mono-cation.[11] In contrast, radical cations of simple thiophenes or their analogues are stable only at low temperatures or their identity inferred from quenching reactions.[12, 13] We were keen to see if we could exploit redox activity and the 'softer' donor properties of the sulfur atoms in methylene-bridged thiophenes to access new transition-metal chemistry and reactivity. As such, we show here that the bis(iminothienyl)methene **L⁻** reacts with metal salts to generate the neutral radical **L˙**, the dicationic radical **L˙²⁺** or the dinuclear copper(I) complex Cu₂I₂(**L˙**) of a ligand-based iminothienyl radical.
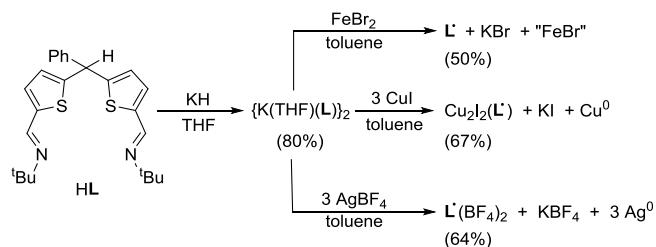
Scheme 1. Synthetic pathway to the monoanionic iminodithiophene K**L** and its redox reactions with metal salts (isolated yields in parentheses).

Studies on the *meso*-C lithiation of dithiophenemethane compounds have found thermodynamic *versus* kinetic selectivity issues along with the formation of *meso*-C coupled products.[14] However, we find that deprotonation of H**L** with KH in THF selectively forms the highly moisture-sensitive potassium salt K**L** as green crystals in high yield (Scheme 1).

The X-ray structure reveals a dimeric structural motif in the solid state (Figure 2). The two imino-thiophene ligands adopt a dinuclear mesocate arrangement at the K centers. The K-S distances appear long (> 3.3 Å), but as no other K-S(thiophene) compound exist no comparisons can be made. The deprotonated ligand shows extended π-conjugation, evident from the planar arrangement of the ligand components linked by the sp² hybridized *meso*-carbon C10; the dihedral angle between iminothienyl planes is 5.9° and the C9-C10 and C10-C17 distances are shortened by 0.1 Å in comparison to the sp³-hybridized H**L** (SI). This unusual dinuclear coordination motif is likely related to the large separation of the imine nitrogen donor

---

[a]   M. Curcio, J. R. Pankhurst, Dr. D. Mignard, Prof. J. B. Love
        EaStCHEM School of Chemistry and School of Engineering
        University of Edinburgh, The King's Buildings
        Edinburgh, EH9 3FJ (UK)
        E-mail: Jason.Love@ed.ac.uk
[b]   Dr. S. Sproules
        WestCHEM School of Chemistry
        University of Glasgow
        Glasgow G12 8QQ (UK)

        Supporting information for this article is given via a link at the end of the document.

atoms (N1···N2 = 7.357(1) Å) as a consequence of incorporating the thiophene heterocycles. This is evidenced by comparison with the X-ray crystal structure of the analogous potassium iminodipyrrin K(L^{N4}) in which the K cation is coordinated to all four N atoms of the ligand, with an imino N1···N4 separation of 5.513(2) Å (Figure S18).
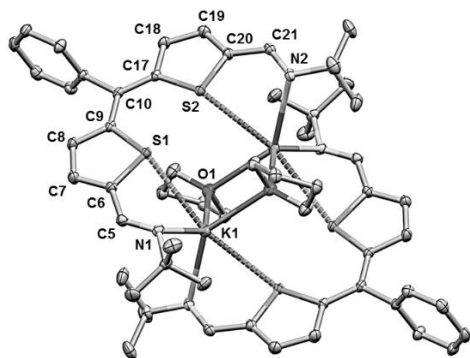

Figure 2. Solid-state structure of K**L**. For clarity, all hydrogen atoms and a molecule of benzene solvent are omitted (displacement ellipsoids are drawn at 50% probability). Selected bond lengths (Å) and angles (°): S1-K1 3.3461(6), N1-K1 2.821(1), N1-C5 1.290(1), S2-K1 3.3676(5), N2-K1 2.852(1), N2-C21 1.289(1), C9-C10-C17 127.3(1), S1-K-N1 58.96(2), S2-K-N2 59.18(2).

The availability of K**L** allowed reactions with transition metal salts to be explored (Scheme 1). The reaction between K**L** and FeBr$_2$ did not lead to the metathesis product FeBr(**L**) but instead results in the neutral, toluene-soluble, metal-free radical **L**•. This highlights the poor coordinating ability of the thiophene ligand compared to its dipyrrin analogue. The radical **L**• is isolated as dichroic yellow/green crystals from toluene and its solid-state structure determined (Figure 3, left), from which it is clear that the *meso*-carbon C10 is sp^2 hybridized with delocalized C9-C10 and C10-C17 bonds. Furthermore, the two iminothienyl planes are coplanar (torsion angle of 2.2°), suggestive of extended π-conjugation across the molecule. The radical nature of **L**• is supported by its fluid-solution EPR spectrum in CH$_3$CN, which shows a resonance at g = 2.0034, consistent with an organic radical (Figure 4). The weakly resolved hyperfine arises from coupling of the unpaired electron to six ^{1}H (I = $^1/_2$) and two ^{14}N (I = 1) nuclei, simulated with A^N = 3.02 × 10^{-4} cm^{-1} and three sets of protons, A^H = 1.43, 1.24, 0.71 × 10^{-4} cm^{-1}, and consistent with the calculated spin-density distribution (Figure 5). EPR spectra of samples diluted in CH$_2$Cl$_2$, toluene and THF, suffer from perturbed molecular tumbling which leads to line broadening that generates featureless signals. While the existence of the radical cations of benzannulated thiophene heterocycles has been probed by trapping with O$_2$,[12] only one example of an isolable neutral thiophene radical has been reported to date by taking advantage of stabilization by delocalization throughout a macrocyclic framework;[11] therefore, to the best of our knowledge, compound **L**• is the first isolable acyclic, neutral thiophene radical.
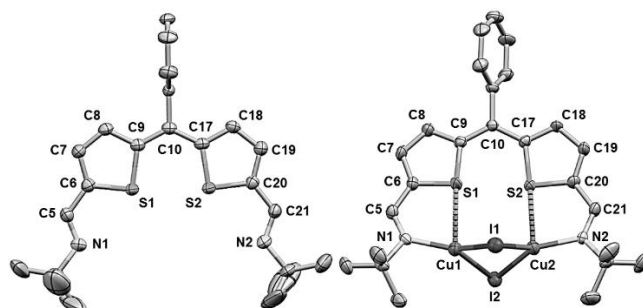

Figure 3. Solid-state structures of **L**• (left) and Cu$_2$I$_2$(**L**•) (right). For clarity, all hydrogen atoms are omitted (displacement ellipsoids are drawn at 50% probability). Selected bond lengths (Å) and angles (°): **L**• N1-C5 1.280(4), C5-C6 1.428(5), S1-C6 1.729(3), S1-C9 1.752(3), C6-C7 1.378(5), C7-C8 1.381(5), C8-C9 1.401(4), C9-C10 1.423(5), C9-C10-C17 126.4(3); Cu$_2$I$_2$(**L**•) S1-Cu1 2.679(2), N1-Cu1 1.982(1), Cu1-I1 2.587(7), Cu1-I2 2.625(9), S2-Cu2 2.689(2), N2-Cu2 1.969(4), Cu2-I1 2.564(6), Cu2-I2 2.587(9), N1-C5 1.283(3), N2-C21 1.290(6), C9-C10-C17 125.8(8), S1-Cu1-N1 79.1(2), S2-Cu2-N2 80.3(2), N1-Cu1-I1 128.7(2), N1-Cu1-I2 129.3(2), Cu1-I1-Cu2 72.72(4), Cu1-I2-Cu2 71.73(4), I1-Cu1-I2 101.29(5), I1-Cu2-I2 102.96(5).

The reaction between K**L** and CuI results in both a precipitate of KI and reduction of Cu(I) to Cu metal but, unlike the reaction with Fe, the metalated product Cu$_2$I$_2$(**L**•) is isolated from toluene as a red powder. The solid-state structure was determined by X-ray crystallography and confirms its dinuclear nature,[15] with each Cu center adopting a distorted trigonal pyramidal geometry with the thienyl-S atom axial and imino-N and bridging-I atoms equatorial (Figure 3, right). The Cu-S distance is within the range (2.336 – 3.014 Å) seen for the five other Cu-thiophene complexes.[16] As with K**L** and **L**•, the *meso*-carbon C10 is sp^2 hybridized with the two iminothienyl fragments essentially coplanar (7.9°). The paramagnetism of Cu$_2$I$_2$(**L**•) could conceivably arise from either the presence of the ligand radical **L**• and two Cu(I) centers, or from an anionic ligand with delocalized Cu(I)/Cu(II) mixed-valence cations. While mixed-valence Cu complexes have been reported and are seen to adopt *pseudo*-tetrahedral geometries in the solid state,[17] the fluid-solution EPR spectrum of Cu$_2$I$_2$(**L**•) shows a resonance at g = 1.9958 that is consistent with a ligand-based radical. The lowering of the g-value compared to **L**• is ascribed to spin-orbit contributions from the copper atoms which reduce all g-values to slightly less than g_e, as described by the frozen-solution spectrum (Figure S8). The lack of hyperfine structure may stem from overlapping coupling to the many spin-active nuclei (^{1}H, ^{14}N, ^{63,65}Cu, ^{127}I) in the system. Interestingly, the EPR spectrum in CH$_3$CN is similar to that of the radical **L**•, showing that the complex is labile in strong donor solvents (Figure S9).

The reaction between K**L** and AgBF$_4$ salt provides the dication **L**•(BF$_4$)$_2$ as the sole paramagnetic red/orange product. In the solid-state structure, **L**•(BF$_4$)$_2$ displays a planar arrangement of atoms, with essentially coplanar thienyl moieties (4.3°) (Figure S17. Note, due to the poor data quality only connectivity can be inferred). Interestingly, one of the BF$_4$ anions is accommodated within the N$_2$S$_2$ molecular cleft and interacts with the imine nitrogen atoms with approximate distances of 2.78 Å (N1···F1) and 2.88 Å (N2···F3). The EPR spectrum of **L**•(BF$_4$)$_2$ is simulated with g = 2.0037, which is identical to **L**•. However, the hyperfine splitting pattern is less congested and the spectral profile was modelled with coupling to the ^{14}N nucleus (A^N = 2.38 × 10^{-4} cm^{-1})

and three protons (A^H = 3.22, 1.10, 0.70 × 10^{-4} cm^{-1}) of *one* iminothienyl arm. The spin-density distribution calculated for **L$^{\bullet2+}$** (Figure 5) corroborates this spectrum, showing spin density on one thiophene-imine arm only due to the twist at the *meso*-carbon atom (dihedral angle 50.9°) in the optimized structure. This calculated structure is different to that seen in the X-ray crystal structure of **L$^{\bullet2+}$** which is planar, presumably due to the presence of the BF$_4^-$ counter-ion which interacts with both imine nitrogen atoms.
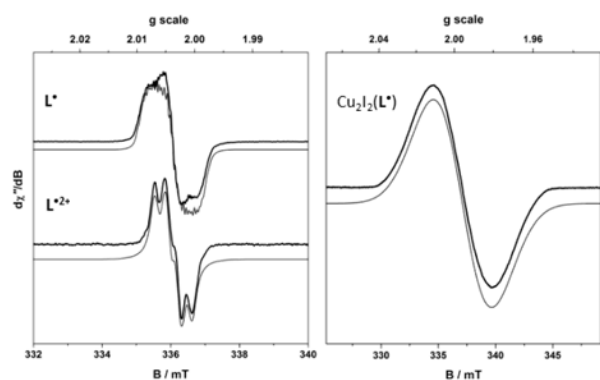
Figure 4. Fluid-solution X-band EPR spectra of radical ligands **L$^{\bullet}$** and **L$^{\bullet}$(BF$_4$)$_2$** in CH$_3$CN (left) and Cu$_2$I$_2$(**L$^{\bullet}$**) in CH$_2$Cl$_2$ (right) at 293 K. Experimental data are depicted by the black trace and simulations by the red trace (simulation parameters are given in the text).

Upon deprotonation of H**L** to form K**L**, an intense band at 654 nm appears (Figure 5), and is similar, although red-shifted, to the HOMO-LUMO transition in related dipyrromethene compounds;[6] the band seen at 295 nm is indicative of re-protonation of K**L** and highlights its sensitivity to water. Oxidation of K**L** to the radical **L$^{\bullet}$** results in a considerable hypsochromic shift of the low-energy absorption band, from 654 to 456 nm, which is explained by an increase in the SOMO(α)-LUMO(α) gap from TD-DFT calculations, from 4.41 keV in K**L** to 5.41 keV in **L$^{\bullet}$**. Incorporation of the dinuclear core in Cu$_2$I$_2$(**L$^{\bullet}$**) leads to the appearance of additional absorption bands, in particular a broad absorption at 826 nm (765 nm in the calculated spectrum) mainly involving the SOMO(β)-LUMO(β) transition. Although the UV-vis spectra are generally well-modeled by TD-DFT simulations, the transitions in Cu$_2$I$_2$(**L$^{\bullet}$**) involve the participation of a multitude of orbitals and cannot be straightforwardly assigned.

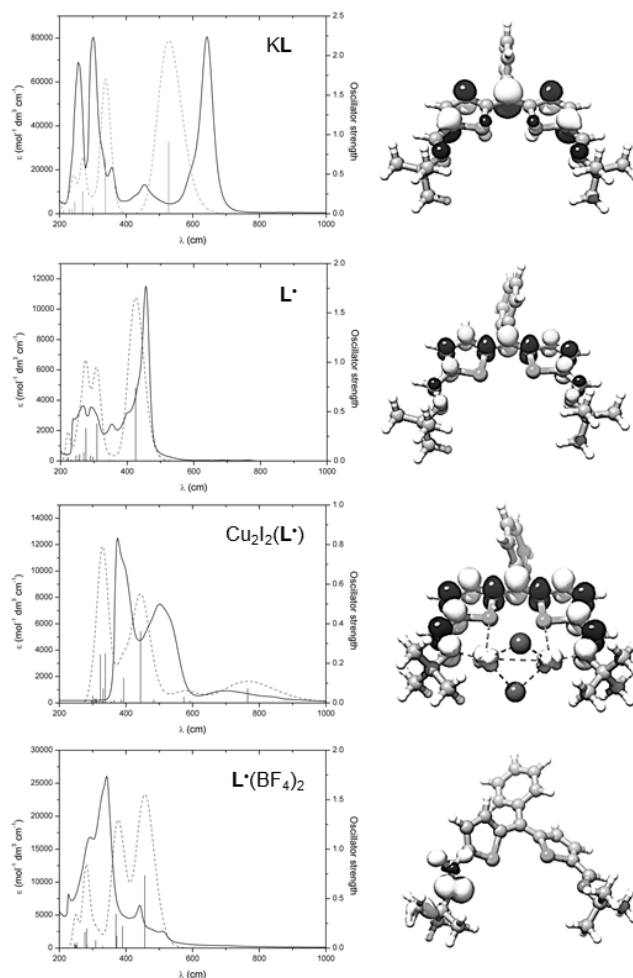**Figure 5.** Left: experimental UV-vis spectra (black trace), TD-DFT calculated spectra (red dashed trace) and oscillators (blue line). Right: DFT calculated HOMO for K**L** and spin-density plots for **L$^{\bullet}$**, Cu$_2$I$_2$(**L$^{\bullet}$**), and **L$^{\bullet2+}$**.

While the cyclic voltammogram (CV) of H**L** displays a single irreversible reduction at E_p^c −1.46 V versus ferrocene (Figure S11), the CV of K**L** consists of two reversible events, with an oxidation at −0.12 V and a reduction at −1.33 V (Figure 6). These are complimentary to the reduction wave at −0.02 V in the CV for **L$^{\bullet}$**, together with another reduction at −1.38 V, assigned by linear-sweep voltammetry; in this case, the data profiles are skewed, indicating quasi-reversibility in the redox properties of **L$^{\bullet}$** which may be due to a lower electrolyte concentration than for K**L** (0.1 M *vs* 0.14 M). In Cu$_2$I$_2$(**L$^{\bullet}$**) the general features of K**L** and **L$^{\bullet}$** are retained, with two similar reductions seen at +0.07 V and −1.00 V; a new irreversible oxidation at +0.83 V is also seen and is tentatively assigned to Cu^{II}/Cu^I oxidation. These data, along with the computed electronic structures, show that the redox reactivity seen in Cu$_2$I$_2$(**L$^{\bullet}$**) is primarily ligand-based.
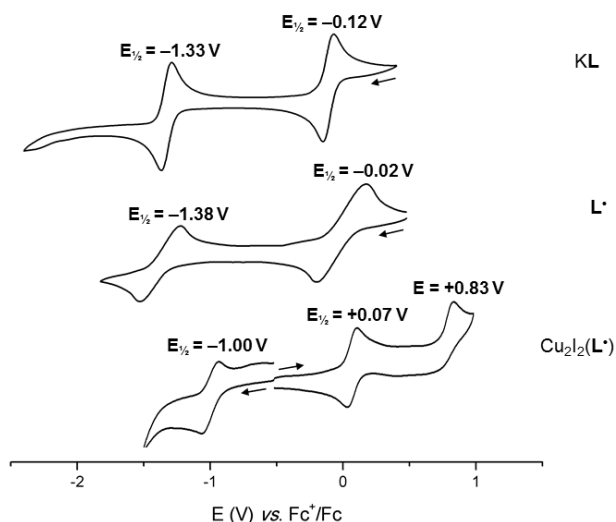
Figure 6. Comparison of CV data for K**L** (green line), **L**· (orange line), and Cu₂I₂(**L**·) (red line); glassy carbon working electrode, platinum gauze counter electrode, silver wire *pseudo*-reference electrode, 100 mV s⁻¹, referenced to Fc⁺/Fc, 1 mM analyte, 0.1 M − 0.14 M [*n*-Bu₄N][PF₆] electrolyte in dry CH₂Cl₂ under N₂.

We have shown that the thiophene analogue of a N-donor expanded dipyrrin exhibits rich radical chemistry, forming the unusual, isolable neutral radical **L**·, its dicopper complex Cu₂I₂(**L**·), and the radical dication **L**·²⁺. The radical chemistry of thiophenes and their complexes is relatively unexplored and primarily limited to examples in which the radical is stabilized within a macrocyclic framework. As such, this work provides the first insight into new thiophene coordination chemistry which, thanks to the redox activity of this ligand framework, could potentially lead to metal complexes with an internal electron reservoir for redox chemical processes.

Acknowledgements

[1]   A. Davison, N. Edelstein, R. H. Holm, A. H. Maki, *Inorg. Chem.* **1963**, *2*, 1227-1232; H. B. Gray, E. Billig, *J. Am. Chem. Soc.* **1963**, *85*, 2019-2020; H. B. Gray, R. Williams, I. Bernal, E. Billig, *J. Am. Chem. Soc.* **1962**, *84*, 3596-3597; G. N. Schrauzer, V. Mayweg, *J. Am. Chem. Soc.* **1962**, *84*, 3221-3221; R. Eisenberg, H. B. Gray, *Inorg. Chem.* **2011**, *50*, 9741-9751; S. Sproules, K. Wieghardt, *Coord. Chem. Rev.* **2010**, *254*, 1358-1382.

[2]   C. T. Lyons, T. D. P. Stack, *Coord. Chem. Rev.* **2013**, *257*, 528-540; W. Kaim, B. Schwederski, *Coord. Chem. Rev.* **2010**, *254*, 1580-1588; A. Krężel, W. Maret, *Biochem. J.* **2007**, *402*, 551-558.

[3]   J. Jacquet, M. Desage-El Murr, L. Fensterbank, *ChemCatChem* **2016**, *8*, 3310-3316; W. Huang, P. L. Diaconescu, *Inorg. Chem.* **2016**, *55*, 10013-10023; D. L. J. Broere, R. Plessius, J. I. van der Vlugt, *Chem. Soc. Rev.* **2015**, *44*, 6886-6915; M. D. Greenhalgh, A. S. Jones, S. P. Thomas, *ChemCatChem* **2015**, *7*, 190-222; O. R. Luca, R. H. Crabtree, *Chem. Soc. Rev.* **2013**, *42*, 1440-1459; R. F. Munha, R. A. Zarkesh, A. F. Heyduk, *Dalton Trans.* **2013**, *42*, 3751-3766; V. Lyaskovskyy, B. de Bruin, *ACS Catalysis* **2012**, *2*, 270-279; V. K. K. Praneeth, M. R. Ringenberg, T. R. Ward, *Angew. Chem. Int. Ed.* **2012**, *51*, 10228-10234; W. Kaim, *Eur. J. Inorg. Chem.* **2012**, *2012*, 343-348; P. J. Chirik, *Inorg. Chem.* **2011**, *50*, 9737-9740; P. J. Chirik, K. Wieghardt, *Science* **2010**, *327*, 794-795.

[4]   V. T. Annibale, D. Song, *RSC Advances* **2013**, *3*, 11432-11449.

[5]   J. R. Pankhurst, T. Cadenbach, D. Betz, C. Finn, J. B. Love, *Dalton Trans.* **2015**, *44*, 2066-2070.

[6]   J. R. Pankhurst, N. L. Bell, M. Zegke, L. N. Platts, C. A. Lamfsus, L. Maron, L. S. Natrajan, S. Sproules, P. L. Arnold, J. B. Love, *Chem. Sci.* **2017**, *8*, 108-116.

[7]   A. Kochem, L. Chiang, B. Baptiste, C. Philouze, N. Leconte, O. Jarjayes, T. Storr, F. Thomas, *Chem. Eur. J.* **2012**, *18*, 14590-14593.

[8]   B. K. Reddy, A. Basavarajappa, M. D. Ambhore, V. G. Anand, *Chem. Rev.* **2017**, *117*, 3420-3443; P. Schweyen, K. Brandhorst, R. Wicht, B. Wolfram, M. Bröring, *Angew. Chem. Int. Ed.* **2015**, *54*, 8213-8216; T. Yoshida, W. Zhou, T. Furuyama, D. B. Leznoff, N. Kobayashi, *J. Am. Chem. Soc.* **2015**, *137*, 9258-9261; Y. Tanaka, Y. Yoneda, K. Furukawa, T. Koide, H. Mori, T. Tanaka, H. Shinokubo, A. Osuka, *Angew. Chem. Int. Ed.* **2015**, *54*, 10908-10911; C. G. Claessens, D. González-Rodríguez, M. S. Rodríguez-Morgade, A. Medina, T. Torres, *Chem. Rev.* **2014**, *114*, 2192-2277; E. T. Hennessy, T. A. Betley, *Science* **2013**, *340*, 591-595; A. Loudet, K. Burgess, *Chem. Rev.* **2007**, *107*, 4891-4932.

[9]   T. Chatterjee, V. S. Shetti, R. Sharma, M. Ravikanth, *Chem. Rev.* **2017**, *117*, 3254-3328.

[10]   S. C. Rasmussen, S. J. Evenson, C. B. McCausland, *Chem. Commun.* **2015**, *51*, 4528-4543.

[11]   T. Y. Gopalakrishna, J. S. Reddy, V. G. Anand, *Angew. Chem. Int. Ed.* **2014**, *53*, 10984-10987.

[12]   A. Wakamiya, T. Nishinaga, K. Komatsu, *Chem. Commun.* **2002**, 1192-1193.

[13]   I. Tabakovic, T. Maki, L. L. Miller, Y. Yu, *Chem. Commun.* **1996**, 1911-1912; P. C. d'Oro, A. Mangini, G. F. Pedulli, P. Spagnolo, M. Tiecco, *Tetrahedron Lett.* **1969**, *10*, 4179-4181.

[14]   K. Singh, A. Sharma, *Tetrahedron* **2010**, *66*, 3682-3686; T. Kawase, T. Enomoto, C. Wei, M. Oda, *Tetrahedron Lett.* **1993**, *34*, 8143-8146.

[15]   T. C. Davenport, T. D. Tilley, *Angew. Chem. Int. Ed.* **2011**, *50*, 12205-12208.

[16]   R. Kia, M. Scholz, P. R. Raithby, S. Techert, *Inorg. Chim. Acta* **2014**, *423, Part A*, 348-357; L.-Z. Chen, G.-F. Han, H.-Y. Ye, H.-W. Hu, *Chin. J. Inorg. Chem.* **2010**, *26*, 2541; A. Doshi, K. Venkatasubbaiah, A. L. Rheingold, F. Jakle, *Chem. Commun.* **2008**, 4264-4266; L. Latos-Grazynski, J. Lisowski, M. M. Olmstead, A. L. Balch, *Inorg. Chem.* **1989**, *28*, 1183-1188; C. R. Lucas, S. Liu, M. J. Newlands, J.-P. Charland, E. J. Gabe, *Can. J. Chem.* **1989**, *67*, 639.

[17]   A. C. Lane, C. L. Barnes, W. E. Antholine, D. Wang, A. T. Fiedler, J. R. Walensky, *Inorg. Chem.* **2015**, *54*, 8509-8517.

Entry for the Table of Contents

stable acyclic radical   π-conjugated anion   binuclear Cu(I) complex
of a ligand radical
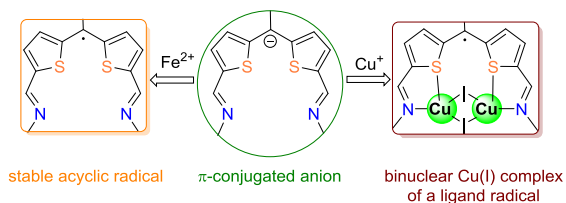
The bis(iminothienyl)methene L^- displays a pronounced redox activity on reactions with metal salts, generating the acyclic neutral radical $L^•$, the neutral $Cu_2I_2(L^•)$ complex of a ligand-centered radical and the metal-free radical dication $L^{•2+}$, all of which are characterised by crystallographic, spectroscopic, and computational techniques.

M. Curcio, J. R. Pankhurst, S. Sproules, D. Mignard, and J. B. Love*

Page No. – Page No.

Triggering redox activity in a thiophene compound: radical stabilization and coordination chemistry

Table of Contents

Experimental

Syntheses of all air- and moisture-sensitive compounds were carried out using standard Schlenk techniques. Vacuum Atmospheres and MBraun glove boxes were used to manipulate and store air- and moisture-sensitive compounds under an atmosphere of dried and deoxygenated dinitrogen. All glassware was dried in an oven at 160 °C, cooled under 10^{-3} mbar vacuum and then purged with nitrogen. All solvents for use with air- and moisture-sensitive compounds were stored in ampoules containing pre-dried 4 Å molecular sieves. Solvents were collected from a Vac Atmospheres solvent tower drying system, where they had been passed over a column of molecular sieves for 24 h prior to collection. They were then degassed prior to use and subsequent storage.

^{1}H-NMR spectra were recorded on a Bruker AVA400 spectrometer operating at 399.90 MHz, a Bruker AVA500 or Bruker PRO500 operating at 500.12 MHz or a Bruker AVA600 spectrometer operating at 599.81 MHz. ^{13}C{^{1}H}-NMR spectra were recorded on a Bruker AVA500 or Bruker PRO500 operating at 125.76 MHz. ^{1}H- and ^{13}C{^{1}H}-NMR spectra are referenced to residual solvent resonances calibrated against an external standard, SiMe$_4$ (= 0 ppm).

Electrochemical measurements were made using an Autolab ECO Chemie PGSTAT potentiostat and the data processed using GPES Manager version 4.9. Experiments were carried out under a flow of N$_2$ in a 10 mL cell. The solution employed was 1 mM of the analyte in THF, with 0.1 M [n-Bu$_4$N][PF$_6$] as the supporting electrolyte. Cyclic voltammograms were recorded for quiescent solutions at variable scan rates between 100-500 mV s^{-1}. The nature of an observed redox process (reduction or oxidation) was determined by linear sweep voltammetry measured for stirred solutions with scan rates between 10-20 mV s^{-1}. The working electrode used was glassy carbon or platinum disc (d = 1 mm), with a platinum gauze counter electrode. Ag/Ag$^+$ pseudo-reference electrode was used with potentials calibrated against [FeCp$_2$]$^{0/+}$.

Elemental analyses were carried out by Mr Stephen Boyer at the London Metropolitan University, measured in duplicate. EPR spectra were recorded on a Bruker ELEXSYS E500 spectrometer. Spectral simulations were performed using Bruker's Xsophe software package.[1] UV-Vis absorption spectra were recorded on a Jasco V-670 spectrophotometer in a 10 mm quartz cuvette, fitted with a Young's tap for air-sensitive compounds.

X-ray crystallographic data were collected at 170 K on an Oxford Diffraction Excalibur diffractometer using graphite monochromated Mo-K radiation equipped with an Eos CCD detector (λ = 0:71073 Å), or at 120 K on a Supernova, Dual, Cu at Zero Atlas diffractometer using Cu-K

radiation (λ = 1:5418 Å). Structures were solved using ShelXT direct methods or intrinsic phasing and refined using a full-matrix least square refinement on $|F|^2$ using ShelXL.[2] All programs were used within the Olex suite.[3] All non-hydrogen atoms refined with anisotropic displacement parameters and H-parameters were constrained to parent atoms and refined using a riding model unless otherwise stated.

DFT calculations were performed using the Gaussian09[4] package on the Eddie server system at the University of Edinburgh. Initial guess geometries were generated from X-ray crystal structures using the Avogadro program (version 1.1.1). All structures discussed in the text were optimised and converged according to the criteria for maximum displacement and maximum force. Frequency calculations were conducted to confirm that the optimised structures represented minimum energy geometries, which were confirmed by having no imaginary frequencies. The "\OPT=NoRaman" and "\FREQ=NoRaman" options were used to improve computational efficiency. TD-DFT calculations were conducted on the first 30 excited states using the SCRF solvent model (\Solvent=Dichloromethane). All optimisation, frequency and TD-DFT calculations were carried out using the CAM-B3LYP functional and 6-311G(d,p) basis set along with the Gen-SDD pseudo potential for I in $Cu_2I_2(L^\bullet)$.[5] Electron Localization Function (ELF) calculations were carried out using the TopMod suite.[6] Molecular orbital surfaces and electron densities from ELF calculations were exported as cubefiles, visualized in UCSF-Chimera[7] and rendered with the Pov-Ray raytracer program.

The reagents thiophene, benzaldehyde, n-BuLi (1.6 M in hexanes), Amberlyst 15®, DMF, tert-butylamine, CuI, $FeBr_2$ and $AgBF_4$ were all used as supplied by Sigma-Aldrich, Fisher Scientific or VWR without further purification.

Compounds 2,10-diformyl-6-phenyl-dithienylmethane **1** and the ligand precursor of the anionic system K(THF)$\mathbf{L^{N4}}$ were synthesized according to published procedures.[8,9]

Synthetic Procedures

Bis(2,2'-thiophene-5,5'-*tert*-butylimino)phenylmethane, HL
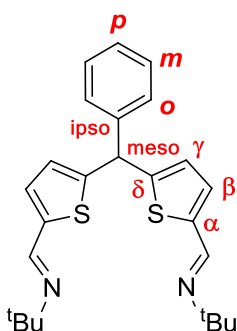
Neat *tert*-butylamine (37.58 mmol, 3.95 mL) was added to **1** (17.89 mmol, 5.59 g) in toluene (125 mL) and the resulting mixture was stirred for 24 h at RT over 4 Å molecular sieves. Filtration through celite and solvent removal provided H**L** as a light brown solid (6.35 g, 84%). ^{1}H NMR (500 MHz, chloroform-*d*) δ 8.27 (d, *J* = 4.5 Hz, 2H, N=C*H*), 7.34-7.28 (m, 4H, *o*-C*H* + *m*-C*H*), 7.28-7.22 (m, 1H, *p*-C*H*), 7.10 (d, *J* = 3.7 Hz, 2H, β-C*H*), 6.82 (d, *J* = 3.7 Hz, 2H, γ-C*H*), 5.77 (s, 1H, *meso*-C*H*), 1.24 (s, 18H, C*H*$_3$). ^{13}C NMR (126 MHz, chloroform-*d*) δ 150.02 (*ipso*-*C*), 148.87 (*C*=N) , 143.31 (α-*C*), 142.61 (δ-*C*), 129.41 (β-*C*), 128.68 (*m*-*C*), 128.42 (*o*-*C*), 127.36 (*p*-*C*), 126.40 (γ-*C*), 57.24 (*C*CH$_3$), 48.52 (*meso*-*C*), 29.71 (*C*H$_3$). Anal. Calcd. for [C$_{25}$H$_{30}$N$_2$S$_2$] C, 71.05; H, 7.15; N, 6.63%; found: C, 70.89; H, 7.08; N, 6.78%. UV-Vis (THF) λ$_{max}$ (ε) 293 nm (28000 dm^3 mol^{-1} cm^{-1}). HRMS-ESI (*m/z*): calcd for [C$_{25}$H$_{30}$N$_2$S$_2$], 422.1850; found 423.1922 [MH]$^+$.

{K(THF)(L)}$_2$
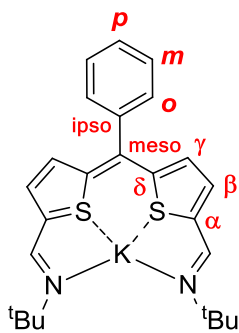
A light brown solution of H**L** (8 mmol, 3.38 g) in THF (40 mL) was added to a suspension of KH (9.2 mmol, 369 mg) in THF (40 mL) and the resulting dark green mixture was stirred under reflux for 24 h. Filtration and layering with hexane afforded over 5 days green crystals of {K(THF)(**L**)}$_2$ (3.2 g, 80%). ^{1}H NMR (500 MHz, THF-*d$_8$*) δ 8.09 (s, 2H, N=C*H*), 7.36-7.20 (m, 4H, *o*-C*H* + *m*-C*H*), 7.16-7.07 (m, 1H, *p*-C*H*), 6.73 (d, *J* = 3.8 Hz, 2H, β-C*H*), 5.79 (d, *J* = 3.6 Hz, 2H, γ-C*H*), 1.19 (d, *J* = 3.2 Hz, 18H, C*H*$_3$). ^{13}C NMR (151 MHz, THF-*d$_8$*) δ 149.58 (δ-*C*), 148.53 (*C*=N), 145.68 (*ipso*-*C*), 132.26 (*o/m*-*C*), 131.58 (β-*C*), 128.21 (*o/m*-*C*), 124.58 (*p*-*C*), 121.88 (α-*C*), 110.32 (γ-*C*), 101.26 (*meso*-*C*), 54.75 (*C*CH$_3$), 30.11 (*C*H$_3$). UV-Vis (THF) λ$_{max}$ (ε) 642 nm (80500 dm^3 mol^{-1} cm^{-1}).

L•
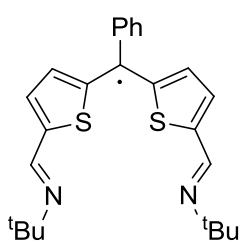
A dark green solution of {K(THF)(**L**)}$_2$ (0.1 mmol, 107 mg) in toluene (5 mL) was added to a toluene suspension of FeBr$_2$ (0.2 mmol, 43 mg) and the resulting mixture was stirred at RT for 16 h, during which it turned light orange. The mixture was then filtered and toluene was removed under reduced pressure to afford a dark orange/brown microcrystalline solid, which was crystallised layering hexane on a THF solution, providing **L•** as dichroic yellow/green crystals (56 mg, 50%). Anal. Calcd. for [C$_{25}$H$_{29}$N$_2$S$_2$] C, 71.21; H, 6.93; N, 6.64%; found: C, 71.13; H, 7.06; N, 6.83%. UV-Vis (THF) λ_{max} (ε) 456 nm (11500 dm^3 mol^{-1} cm^{-1}). HRMS (MALDI) (*m/z*): calcd for [C$_{25}$H$_{29}$N$_2$S$_2$], 421.1778; found 421.1723 [M]$^-$.

Cu$_2$I$_2$(L•)
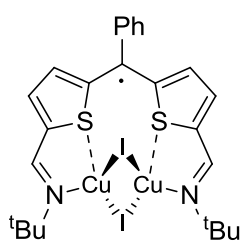
A dark green solution of {K(THF)(**L**)}$_2$ (0.1 mmol, 107 mg) in toluene (5 mL) was added to a toluene suspension of CuI (0.6 mmol, 114 mg) and the resulting mixture was stirred at RT for 16 h, during which a dark precipitate was formed. Toluene was removed by filtration and the residue dissolved in DCM and filtered to remove KI, resulting in a red solution. Removal of the solvent under reduced pressure provided Cu$_2$I$_2$(**L•**) as a dark red solid (109 mg, 67%). Anal. Calcd. for [C$_{25}$H$_{29}$N$_2$S$_2$Cu$_2$I$_2$] C, 37.41; H, 3.64; N, 3.49%; found: C, 37.28; H, 3.89; N, 3.37%. UV-Vis (THF) λ_{max} (ε) 497 (7500), 379 nm (12100 dm^3 mol^{-1} cm^{-1}).

L•(BF$_4$)$_2$
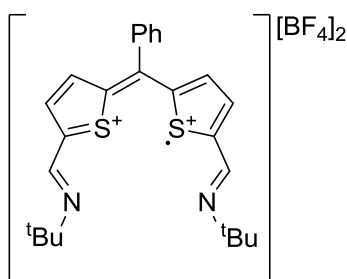
A dark green solution of {K(THF)(**L**)}$_2$ (0.25 mmol, 266 mg) in toluene (5 mL) was added to a toluene (5 mL) suspension of AgBF$_4$ (1.5 mmol, 292 mg) and the resulting mixture was stirred at RT for 16 h, during which a dark precipitate was formed. The solvent was removed by filtration and the residue washed with additional toluene (2 x 2 mL), then dissolved in DCM and filtered resulting in a red/orange solution. Removal of the solvent under reduced pressure provided **L•**(BF$_4$)$_2$ as a brown solid (193 mg, 64%). Anal. Calcd. for [C$_{25}$H$_{29}$B$_2$F$_8$N$_2$S$_2$] C, 50.44; H, 4.91; N, 4.71%; found: C, 50.59; H, 4.77; N, 4.88%. UV-Vis (DCM) λ_{max} (ε) 342 nm (26000 dm^3 mol^{-1} cm^{-1}).

K(THF)L^{N4}
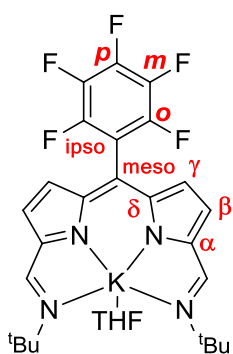
A light brown solution of the dipyrrin precursor HL^{N4}[9] (0.1 mmol, 107 mg) in THF (2 mL) was added to a THF suspension (2 mL) of KH (0.6 mmol, 114 mg) and the resulting mixture was stirred at RT for 30 min, during which the solution turned dark purple. Excess KH was separated by filtration and the solvent was removed under reduced pressure affording a microcrystalline dark purple solid, which was layered with hexane and left at -30°C to provide K(THF)L^{N4} as yellow/green crystals (118 mg, 73%). ^{1}H NMR (400 MHz, THF-d_8) δ = 8.28 (s, 2H, N=CH), 6.51 (d, J=3.9 Hz, 2H, β-CH), 6.40 (d, J=3.7 Hz, 2H, γ-CH), 1.30 (s, 18H, CCH_3). ^{13}C NMR (126 MHz, THF-d_8) δ = 159.55 (ipso-C), 154.04 (N=C), 145.88 (dm, J=126 Hz, Ar^{F5}), 145.74 (δ-C), 141.01 (dm, J=126 Hz, Ar^{F5}), 138.00 (dm, J=126 Hz, Ar^{F5}), 133.30 (α-C), 130.62 (γ-C), 121.32 (β-C), 118.33 (meso-C), 57.63 (CCH$_3$), 30.22 (CH$_3$). ^{19}F NMR (471 MHz, THF-d_8) δ = -143.92 (dd, J=23.3, 6.4, 2F), -160.71 (t, J=20.4, 1F), -167.03 – -167.86 (m, 2F). Anal. Calcd. for [C$_{25}$H$_{29}$N$_4$K] C, 70.71; H, 6.88; N, 13.19%; found: C, 70.55; H, 6.81; N, 13.43%. UV-Vis (THF) λ$_{max}$ (ε) 579 (50000), 299 nm (33300 dm^3 mol^{-1} cm^{-1}).

NMR Spectroscopic Data
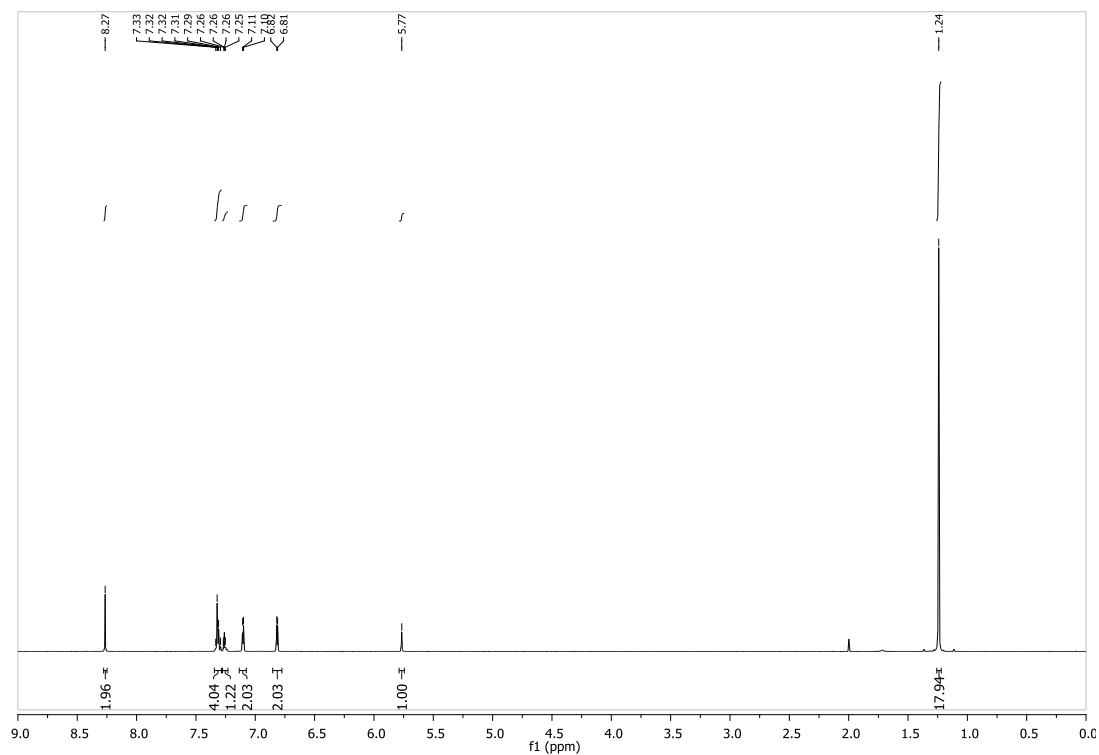
Figure S1. ^{1}H NMR spectrum of H**L** (500 MHz, Chloroform-*d*).
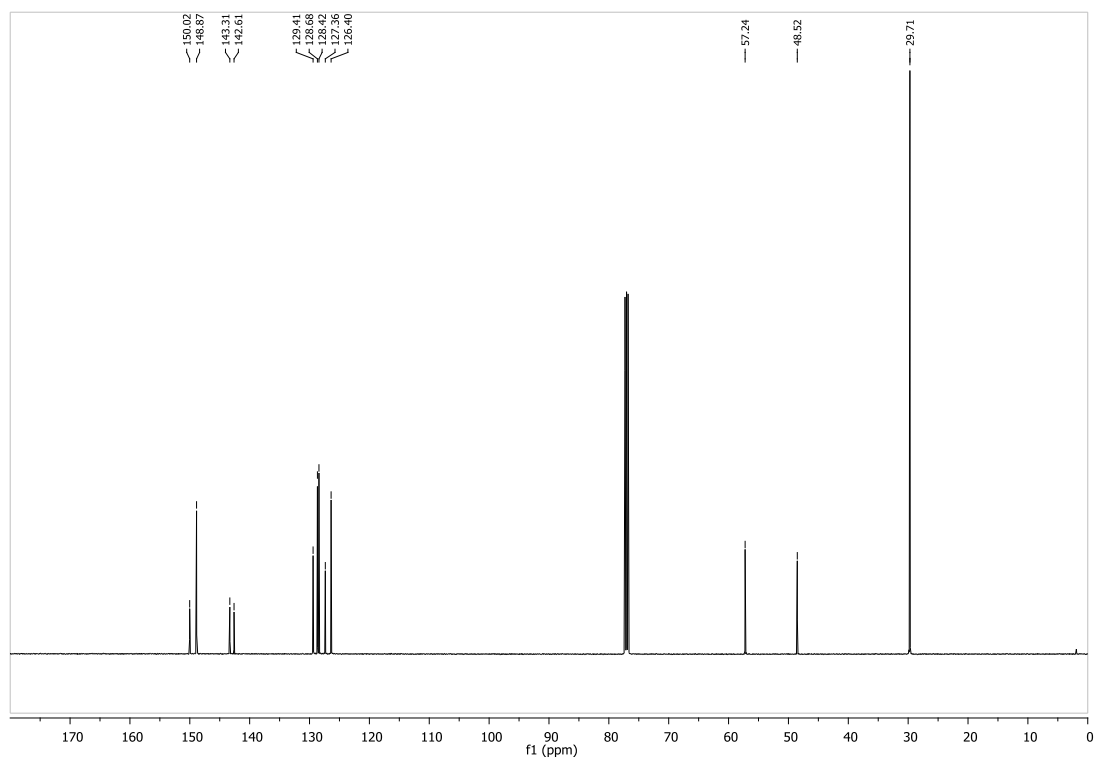
Figure S2. ^{13}C NMR spectrum of H**L** (151 MHz, Chloroform-*d*).
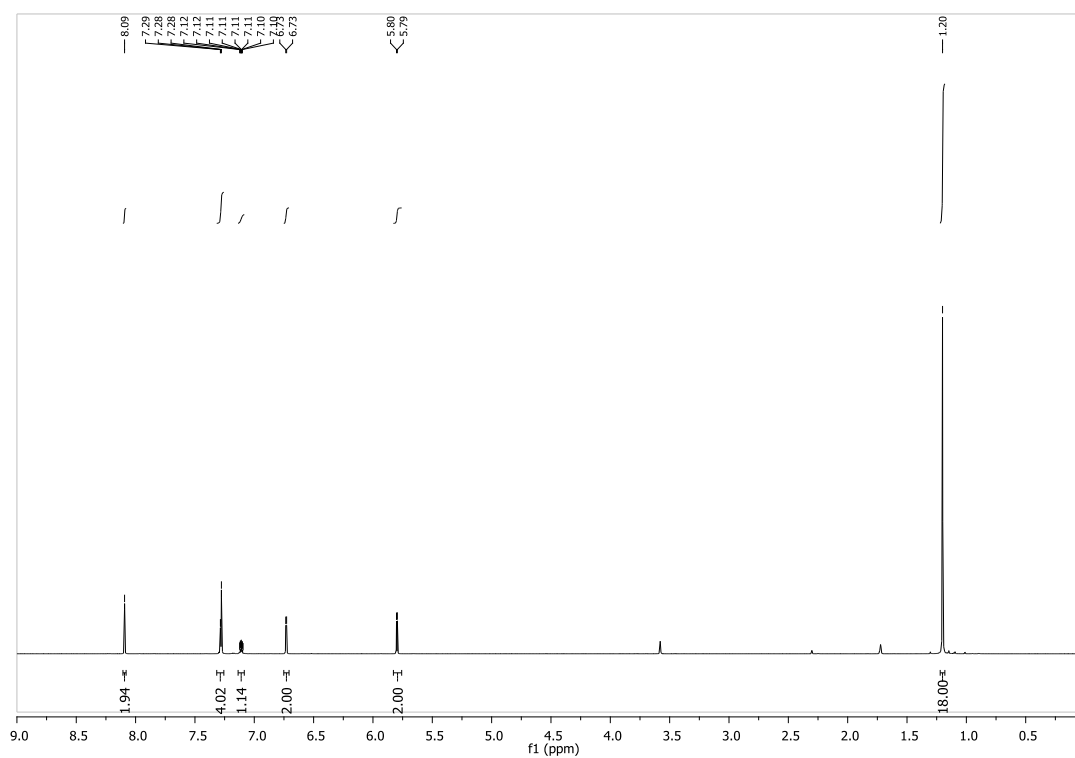
Figure S3. ^{1}H NMR spectrum of {K(THF)(**L**)}$_2$ (600 MHz, THF-d_8).
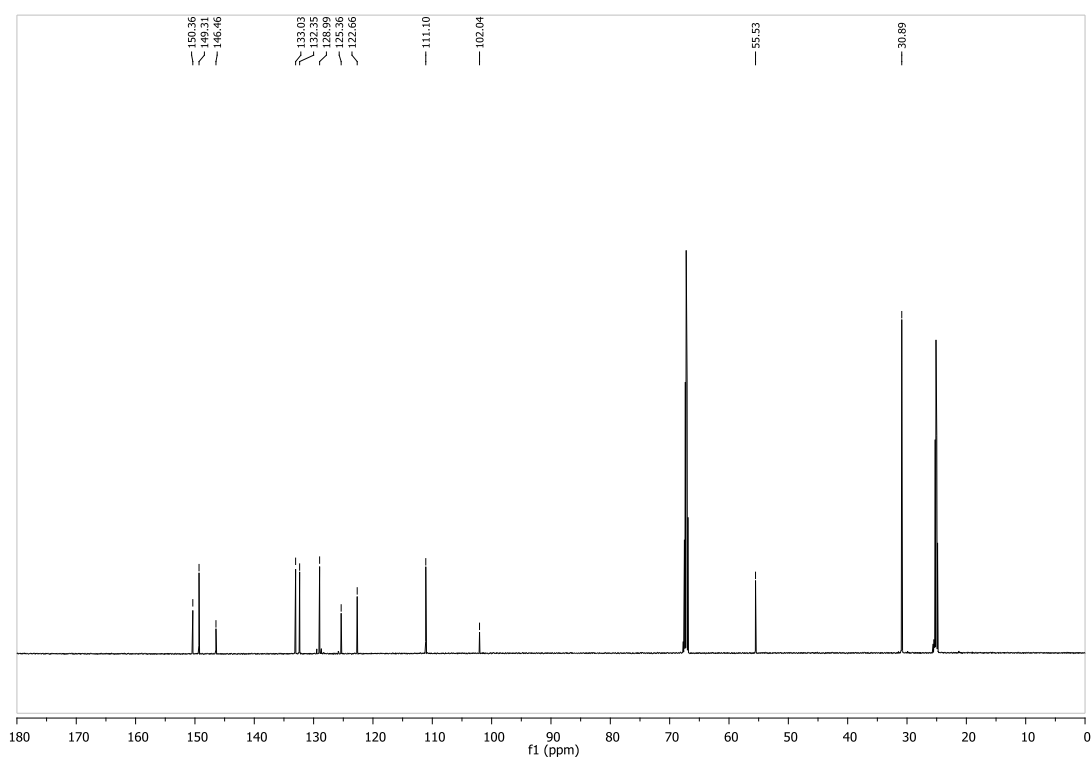
Figure S4. ^{13}C NMR spectrum of {K(THF)(**L**)}$_2$ (151 MHz, THF-d_8).
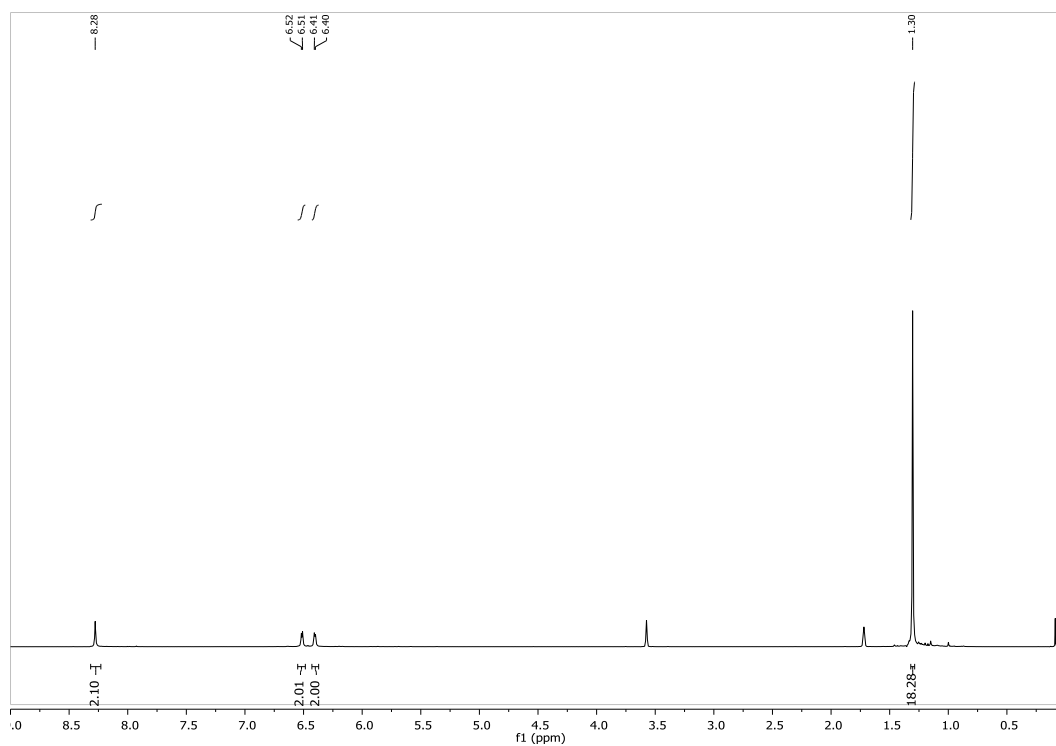
Figure S5. ^{1}H NMR spectrum of **KL^{N4}** (400 MHz, THF-d_8).
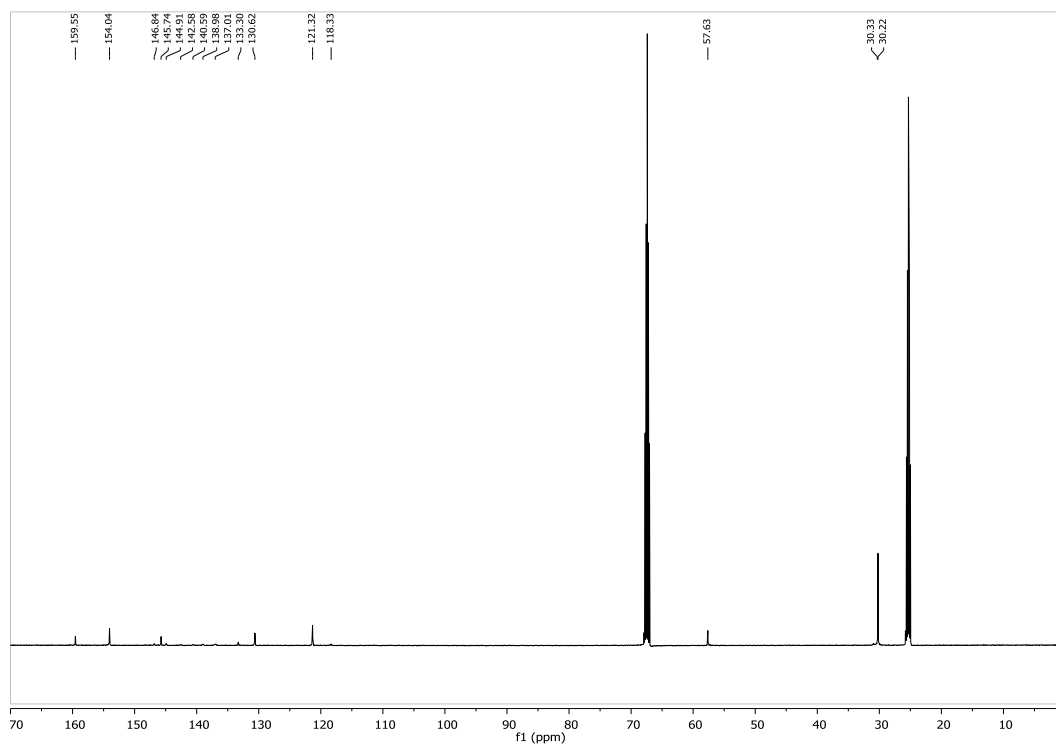
Figure S6. ^{13}C NMR spectrum of **KL^{N4}** (126 MHz, THF-d_8).
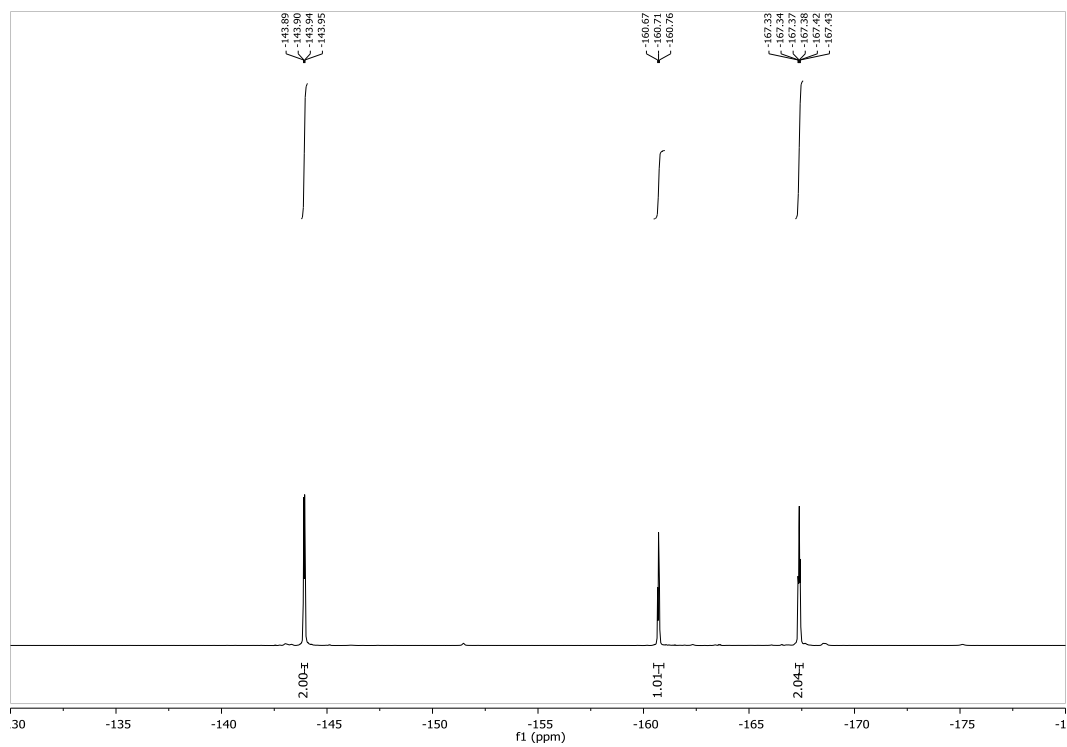
Figure S7. ^{19}F NMR spectrum of **KL**$^{\text{N4}}$ (471 MHz, THF-d_8).

EPR Spectroscopic Data
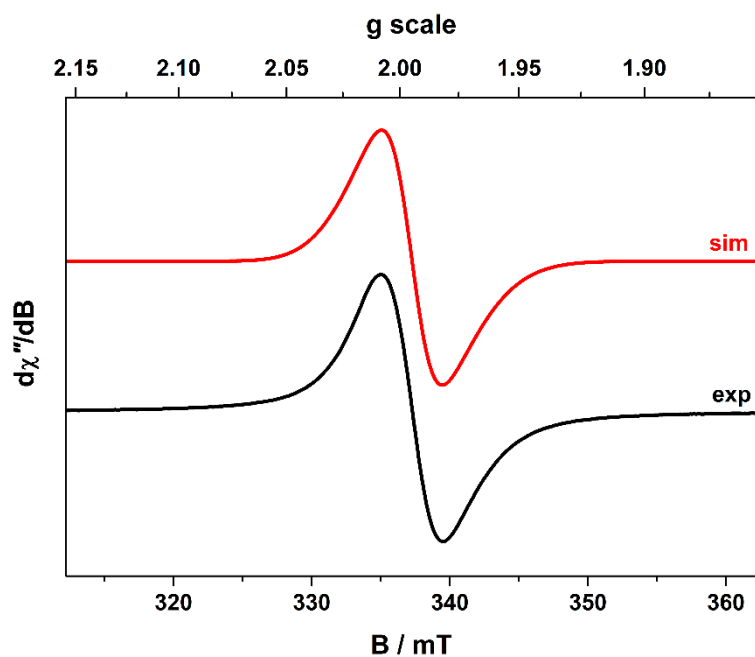
Figure S8. X-band EPR spectrum of $Cu_2I_2(\mathbf{L^{\cdot}})$ recorded in CH_2Cl_2/THF solution at 140 K (experimental conditions: frequency, 9.4162 GHz; power, 0.63 mW; modulation, 0.2 mT). Experimental data are represented by the black line; simulation is depicted by the red trace: $g = (2.001, 1.995, 1.985)$.
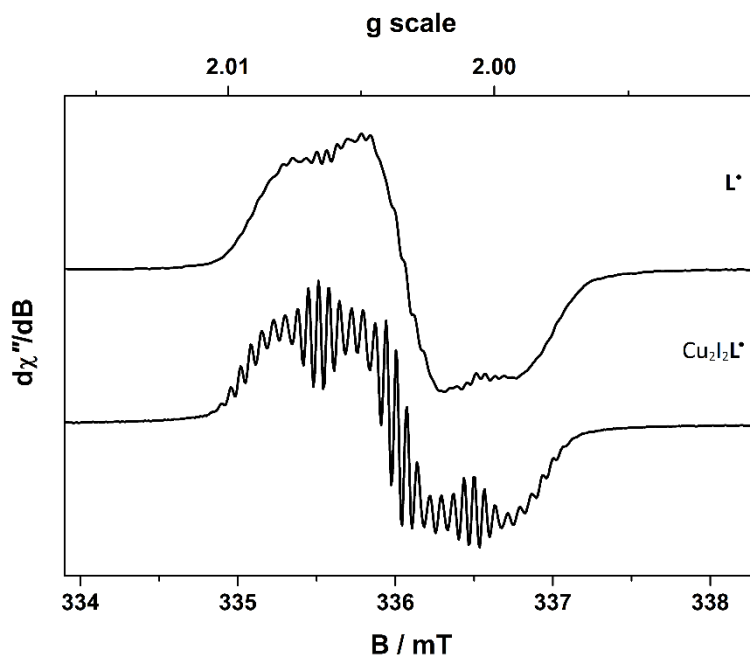
Figure S9. Comparison of the X-band EPR spectra $\mathbf{L^{\cdot}}$ (top) and $Cu_2I_2(\mathbf{L^{\cdot}})$ recorded in acetonitrile at 293 K (experimental conditions: frequency, 9.42 GHz; power, 6.3 mW; modulation, 0.05 mT).

UV-vis Spectroscopic Data
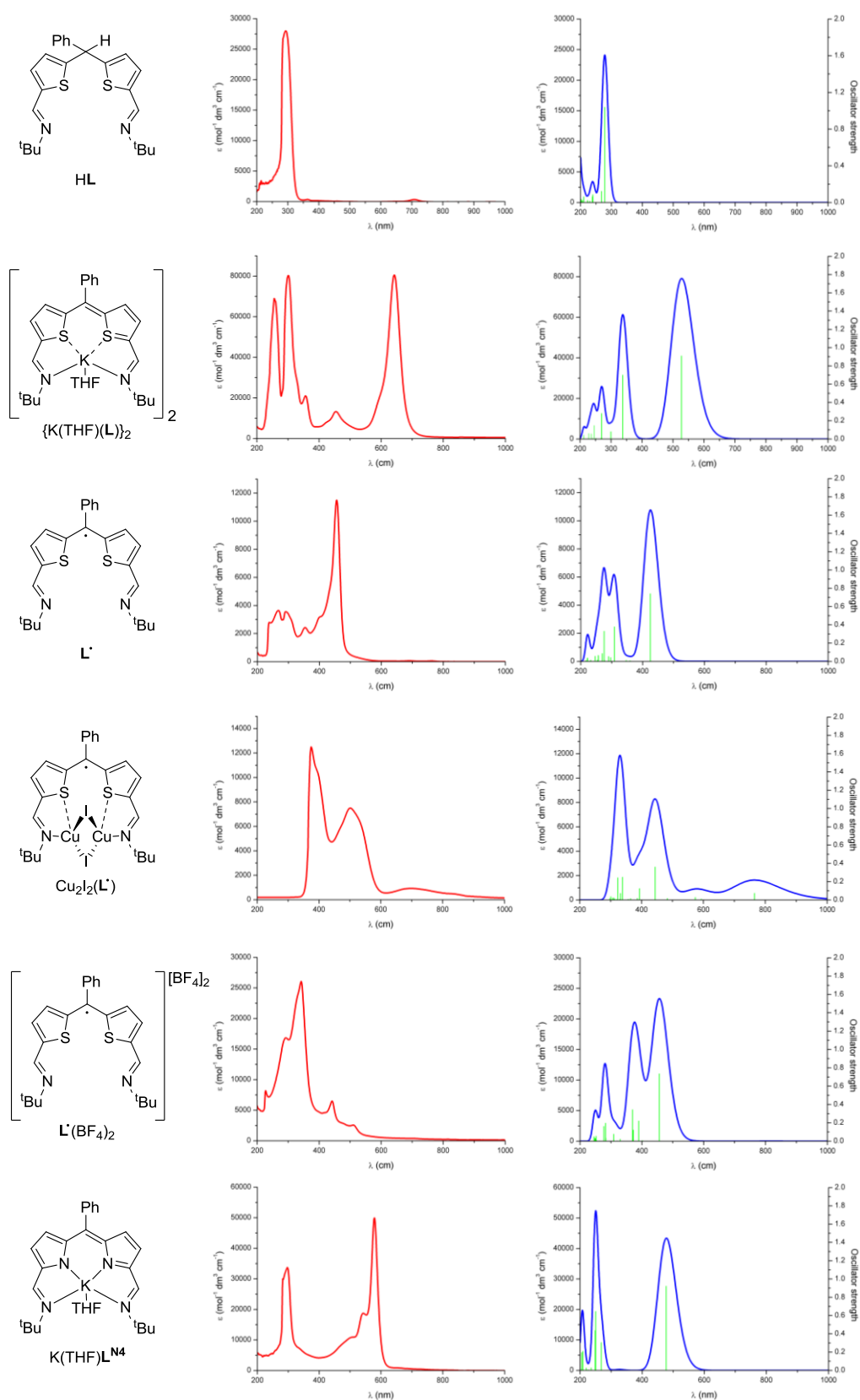
Figure S10. Experimental UV-vis spectra (red trace), TD-DFT calculated spectra (blue trace) and oscillators (green line) of the iminoheterocyclic compounds.

Electrochemical data
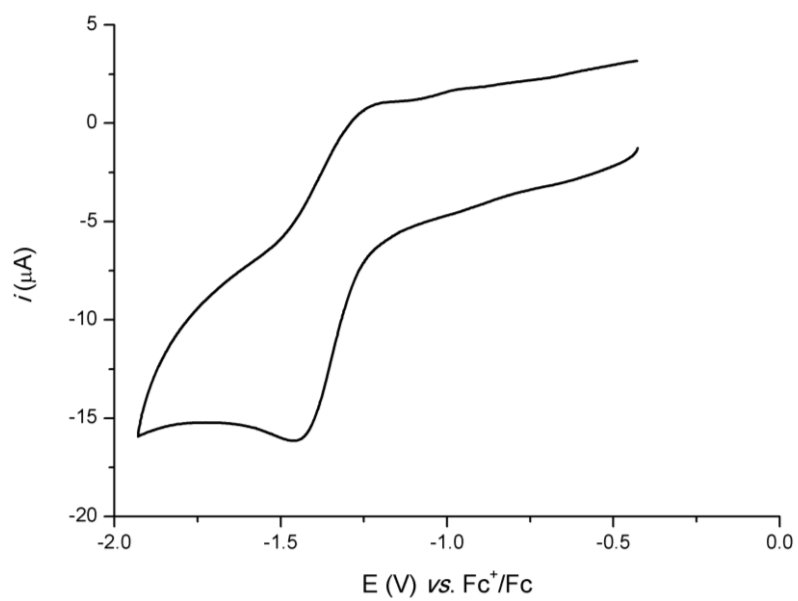
Figure S11. Cyclic voltammogram of H**L** (1 mM H**L**, 0.1 M [n-Bu$_4$N][PF$_6$]).
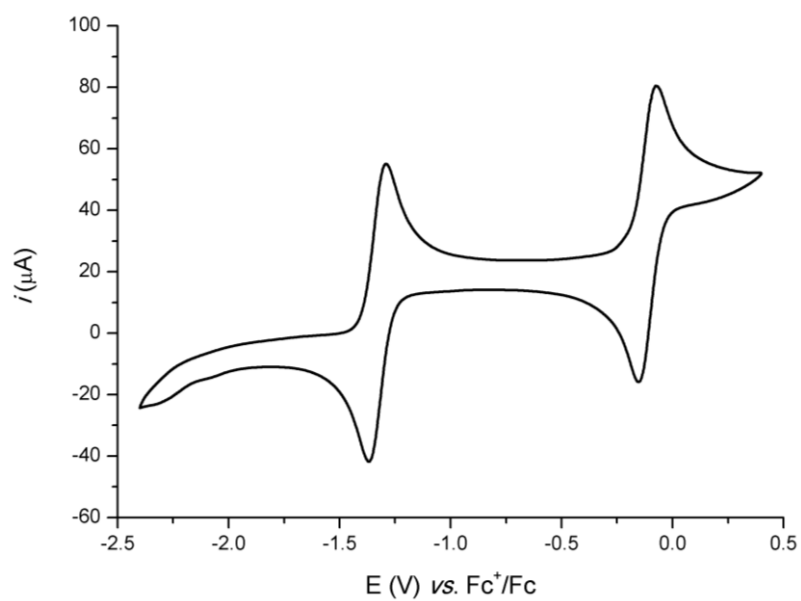
Figure S12. Cyclic voltammogram of {K(THF)(**L**)}$_2$ (1 mM {K(THF)(**L**)}$_2$, 0.1 M [n-Bu$_4$N][PF$_6$]).
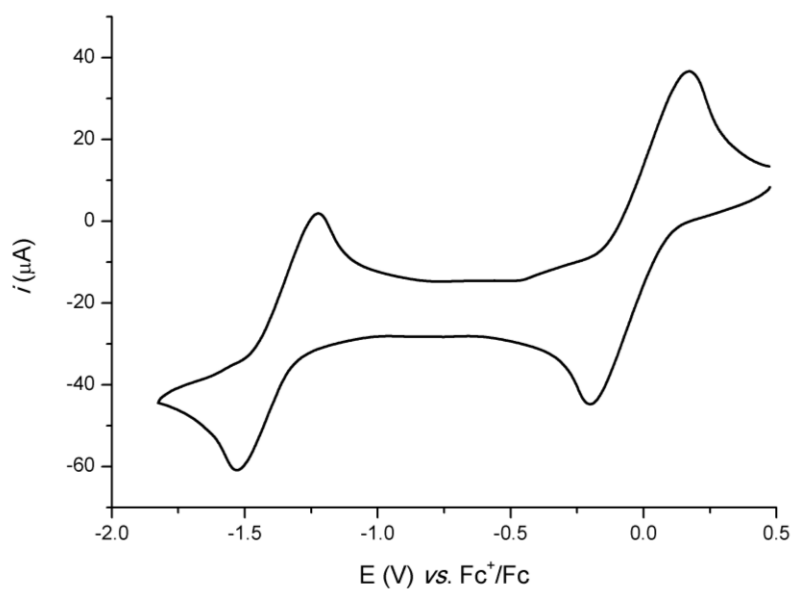
Figure S13. Cyclic voltammogram of **L**$^•$ (1 mM **L**$^•$, 0.1 M [*n*-Bu$_4$N][PF$_6$]).
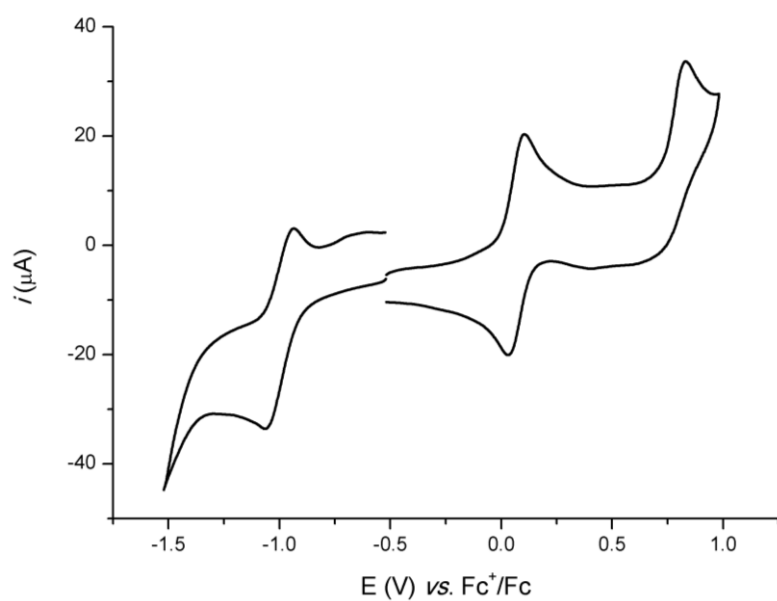
Figure S14. Cyclic voltammogram of Cu$_2$I$_2$(**L**$^•$) (1 mM Cu$_2$I$_2$(**L**$^•$), 0.1 M [*n*-Bu$_4$N][PF$_6$]).
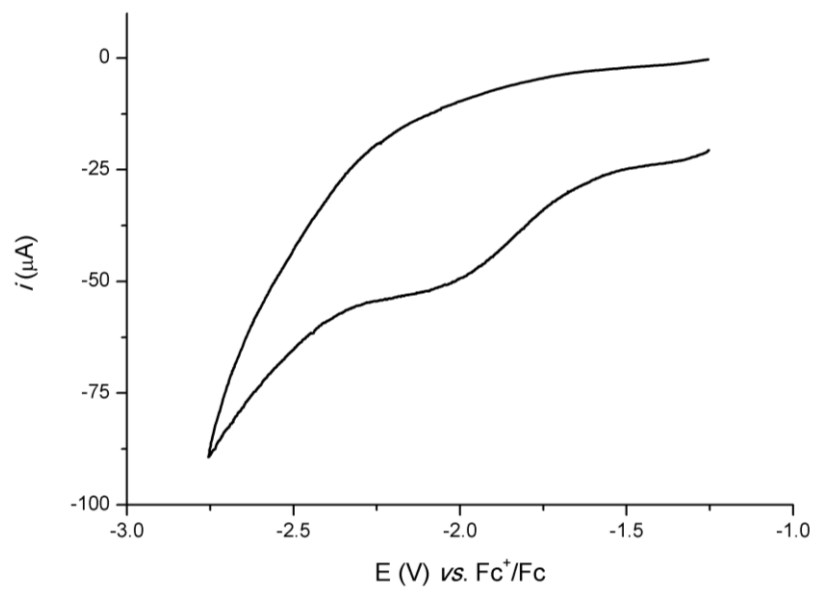
Figure S15. Cyclic voltammogram of **L**ˑ(BF$_4$)$_2$ (1 mM **L**ˑ(BF$_4$)$_2$, 0.1 M [n-Bu$_4$N][PF$_6$]).

Crystallographic Data
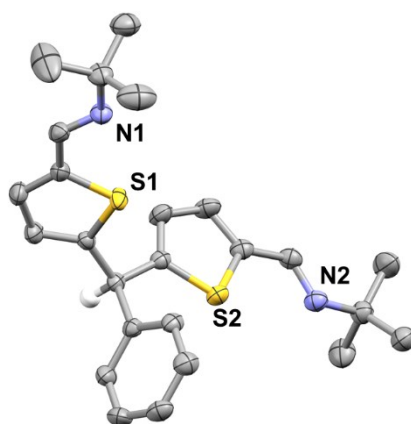
Figure S16. Solid-state structure for **HL** (CCDC 1542226). For clarity, all hydrogen atoms except for the *meso* one are omitted (displacement ellipsoids are drawn at 50% probability).
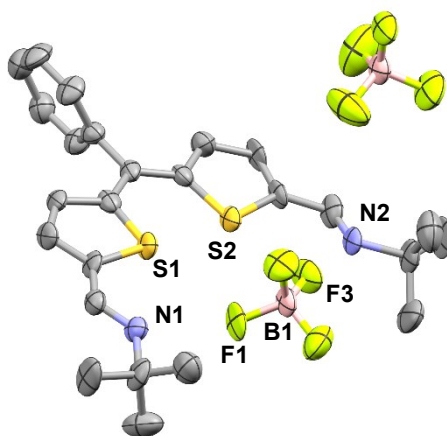

Figure S17. Solid-state structure for **L˙**(BF$_4$)$_2$ (CCDC 1542230). For clarity, all hydrogen atoms and a molecule of dichloromethane are omitted (displacement ellipsoids are drawn at 50% probability). Selected distances (Å): N1-F1 2.780(9), N2-F3 2.884(1).
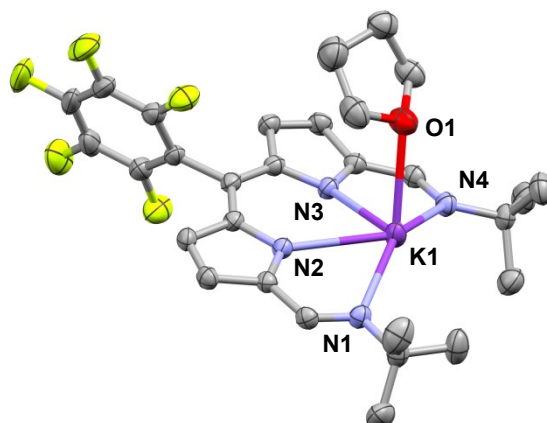
Figure S18. Solid-state structure for K(THF)$\mathbf{L^{N4}}$ (CCDC 1542231). For clarity, all hydrogen atoms are omitted (displacement ellipsoids are drawn at 50% probability). Selected distances (Å): N1-K1 2.868(2), N2-K1 2.730(2), N3-K1 2.698(1), N4-K1 2.813(2), N1-N4 5.513(2).

Table S1. Crystal structure refinement parameters for H**L** and {K(THF)(**L**)}₂.

	HL (CCDC 1542226)	{K(THF)(L)}₂ (CCDC 1542227)
Chemical formula	$C_{25}H_{30}N_2S_2$	$C_{29}H_{37}KN_2OS_2 \cdot C_6H_6$
M_r	422.63	610.93
Crystal system, space group	Monoclinic, $P2_1/n$	Orthorhombic, $Pbca$
Temperature (K)	170	120
a, b, c (Å)	14.1650 (4), 5.96736 (15), 27.6601 (7)	15.8437 (2), 18.2093 (3), 22.8804 (4)
β (°)	96.238 (2)	
V (Å³)	2324.19 (11)	6601.07 (18)
Z	4	8
Radiation type	Mo $K\alpha$	Mo $K\alpha$
μ (mm⁻¹)	0.24	0.32
Crystal size (mm)	$0.31 \times 0.26 \times 0.08$	$0.50 \times 0.38 \times 0.21$
Data collection		
Diffractometer	Xcalibur, Eos	SuperNova, Dual, Cu at zero, Atlas
Absorption correction	Multi-scan *CrysAlis PRO*, Agilent Technologies, Version 1.171.37.34 (release 22-05-2014 CrysAlis171 .NET) (compiled May 22 2014, 16:03:01) Empirical absorption correction using spherical harmonics, implemented in SCALE3 ABSPACK scaling algorithm. Empirical absorption correction using spherical harmonics, implemented in SCALE3 ABSPACK scaling algorithm.	Multi-scan *CrysAlis PRO*, Agilent Technologies, Version 1.171.37.35e (release 07-10-2014 CrysAlis171 .NET) (compiled Oct 7 2014, 17:20:27) Empirical absorption correction using spherical harmonics, implemented in SCALE3 ABSPACK scaling algorithm. Empirical absorption correction using spherical harmonics, implemented in SCALE3 ABSPACK scaling algorithm.
T_{min}, T_{max}	0.858, 1.000	0.643, 1.000
No. of measured, independent and observed [$I > 2\sigma(I)$] reflections	32568, 4074, 3301	134201, 10289, 9265
R_{int}	0.055	0.041
$(\sin \theta/\lambda)_{max}$ (Å⁻¹)	0.595	0.730
Refinement		
$R[F^2 > 2\sigma(F^2)]$, $wR(F^2)$, S	0.049, 0.149, 1.04	0.039, 0.137, 1.08
No. of reflections	4074	10289
No. of parameters	268	376
H-atom treatment	H-atom parameters constrained	H-atom parameters constrained
$\Delta\rangle_{max}$, $\Delta\rangle_{min}$ (e Å⁻³)	0.31, -0.24	0.41, -0.44

Table S2. Crystal structure refinement parameters for **L˙** and Cu$_2$I$_2$(**L˙**).

	L˙ (CCDC 1542228)	Cu$_2$I$_2$(**L˙**) (CCDC 1542229)
Chemical formula	C$_{25}$H$_{29}$N$_2$S$_2$	C$_{25}$H$_{29}$Cu$_2$I$_2$N$_2$S$_2$
M_r	423.06	802.50
Crystal system, space group	Triclinic, $P\bar{1}$	Monoclinic, $P2_1$
Temperature (K)	170	170
a, b, c (Å)	5.7800 (3), 11.1718 (5), 19.2205 (9)	8.7699 (2), 13.2069 (3), 12.5335 (3)
α, β, γ (°)	98.344 (4), 97.954 (4), 96.777 (4)	-, 103.152 (3), -
V (Å^3)	1204.04 (10)	1413.58 (7)
Z	2	2
Radiation type	Mo $K\alpha$	Mo $K\alpha$
μ (mm^{-1})	0.23	3.85
Crystal size (mm)	0.53 × 0.13 × 0.05	0.34 × 0.08 × 0.03
Data collection		
Diffractometer	Xcalibur, Eos	Xcalibur, Eos
Absorption correction	Multi-scan *CrysAlis PRO*, Agilent Technologies, Version 1.171.37.34 (release 22-05-2014 CrysAlis171 .NET) (compiled May 22 2014,16:03:01) Empirical absorption correction using spherical harmonics, implemented in SCALE3 ABSPACK scaling algorithm. Empirical absorption correction using spherical harmonics, implemented in SCALE3 ABSPACK scaling algorithm.	Analytical *CrysAlis PRO*, Agilent Technologies, Version 1.171.37.34 (release 22-05-2014 CrysAlis171 .NET) (compiled May 22 2014,16:03:01) Analytical numeric absorption correction using a multifaceted crystal model based on expressions derived by R.C. Clark & J.S. Reid. (Clark, R. C. & Reid, J. S. (1995). Acta Cryst. A51, 887-897) Empirical absorption correction using spherical harmonics, implemented in SCALE3 ABSPACK scaling algorithm.
T_{min}, T_{max}	0.848, 1.000	0.772, 0.971
No. of measured, independent and observed [$I > 2\sigma(I)$] reflections	17368, 4095, 3126	22834, 5578, 4746
R_{int}	0.048	0.063
$(\sin\theta/\lambda)_{max}$ (Å^{-1})	0.588	0.617
Refinement		
$R[F^2 > 2\sigma(F^2)]$, $wR(F^2)$, S	0.065, 0.192, 1.26	0.040, 0.072, 1.00
No. of reflections	4095	5578
No. of parameters	269	304
No. of restraints		1

H-atom treatment	H-atom parameters constrained	H-atom parameters constrained
$\Delta\rangle_{max}$, $\Delta\rangle_{min}$ (e Å^{-3})	1.02, -0.33	0.74, -0.57
Absolute structure		Flack x determined using 1895 quotients [(I+)-(I-)]/[(I+)+(I-)] (Parsons, Flack and Wagner, Acta Cryst. B69 (2013) 249-259).
Absolute structure parameter		-0.020 (16)

Table S3. Crystal structure refinement parameters for **L˙**(BF$_4$)$_2$ and K(THF)**L^{N4}**.

	L˙(BF$_4$)$_2$ (CCDC 1542230)	K(THF)**L^{N4}** (CCDC 1542231)
Chemical formula	C$_{25}$H$_{29}$N$_2$S$_2$·CH$_2$Cl$_2$·2(BF$_4$)	C$_{58}$H$_{64}$F$_{10}$K$_2$N$_8$O$_2$
M_r	680.17	1173.37
Crystal system, space group	Monoclinic, $P2_1/c$	Monoclinic, $P2_1/n$
Temperature (K)	293	170
a, b, c (Å)	9.2047 (12), 28.642 (4), 13.2579 (16)	11.8073 (4), 10.3062 (4), 24.1283 (9)
α, β, γ (°)	109.040 (14)	99.897 (3)
V (Å^3)	3304.1 (8)	2892.44 (19)
Z	4	2
Radiation type	Mo $K\alpha$	Mo $K\alpha$
μ (mm^{-1})	0.39	0.25
Crystal size (mm)	0.34 × 0.19 × 0.09	0.98 × 0.48 × 0.27
Data collection		
Diffractometer	Xcalibur, Eos	Xcalibur, Eos
Absorption correction	Analytical *CrysAlis PRO*, Agilent Technologies, Version 1.171.37.35 (release 13-08-2014 CrysAlis171 .NET) (compiled Aug 13 2014,18:06:01) Analytical numeric absorption correction using a multifaceted crystal model based on expressions derived by R.C. Clark & J.S. Reid. (Clark, R. C. & Reid, J. S. (1995). Acta Cryst. A51, 887-897) Empirical absorption correction using spherical harmonics, implemented in SCALE3 ABSPACK scaling algorithm.	Analytical *CrysAlis PRO* 1.171.38.42b (Rigaku Oxford Diffraction, 2015) Analytical numeric absorption correction using a multifaceted crystal model based on expressions derived by R.C. Clark & J.S. Reid. (Clark, R. C. & Reid, J. S. (1995). Acta Cryst. A51, 887-897) Empirical absorption correction using spherical harmonics, implemented in SCALE3 ABSPACK scaling algorithm.
T_{min}, T_{max}	0.994, 0.998	0.864, 0.958
No. of measured, independent and observed [$I > 2\sigma(I)$]	42080, 5256, 3729	33565, 5909, 4685

reflections		
R_{int}	0.145	0.038
$(\sin \theta/\lambda)_{max}$ (Å^{-1})	24.1	0.625
Refinement		
$R[F^2 > 2\sigma(F^2)]$, $wR(F^2)$, S	0.147, 0.358, 1.08	0.042, 0.105, 1.04
No. of reflections	5256	5909
No. of parameters	385	371
No. of restraints		
H-atom treatment	H-atom parameters constrained	H atoms treated by a mixture of independent and constrained refinement
	$w = 1/[\sigma^2(F_o^2) + (0.105P)^2 + 42.480P]$ where $P = (F_o^2 + 2F_c^2)/3$	
$\Delta\rangle_{max}$, $\Delta\rangle_{min}$ (e Å^{-3})	0.77, -0.57	0.31, -0.30

Computational data
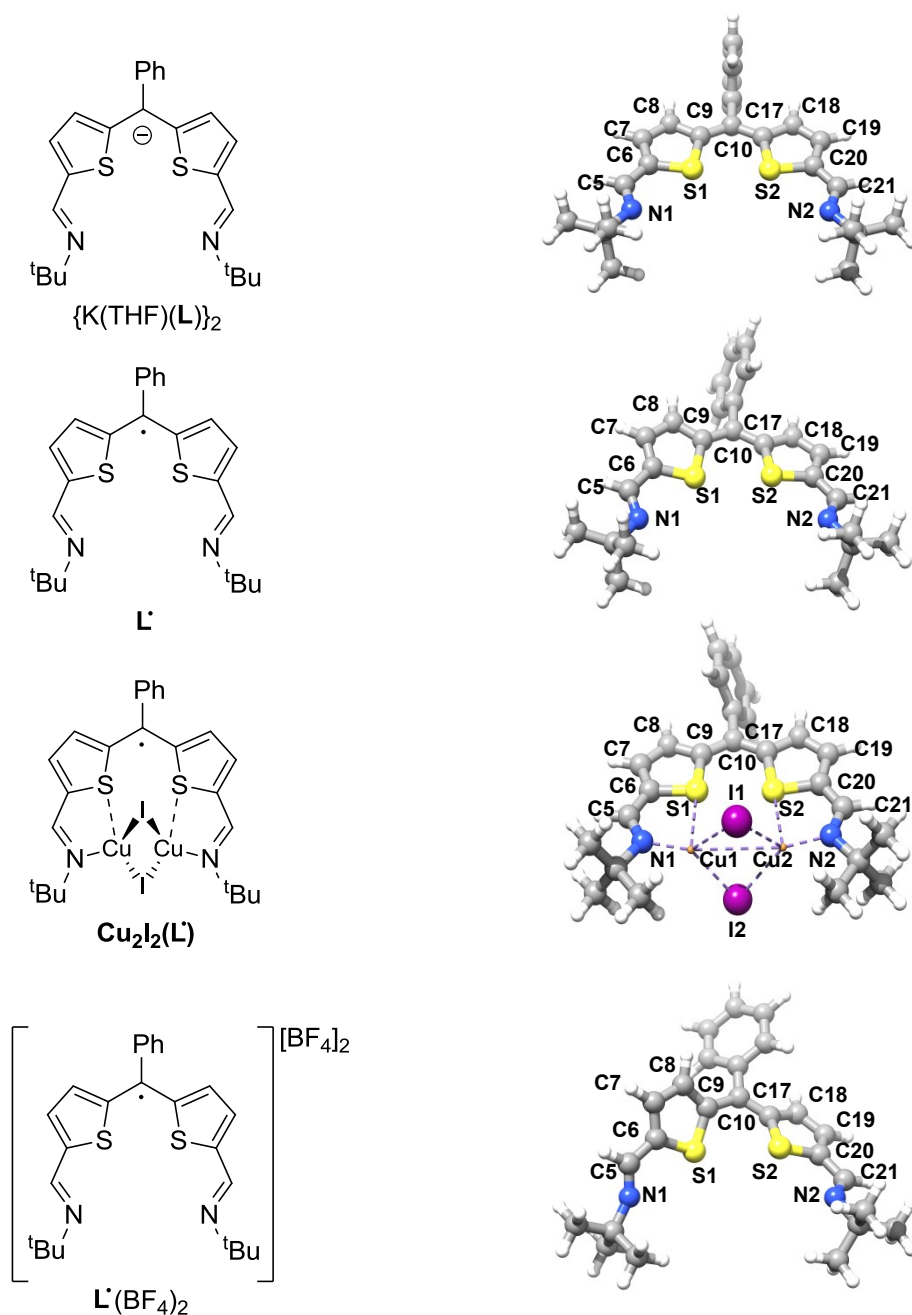
Figure S19. Optimized geometric coordinates of the iminothienyl compounds. Selected distances (Å) and angles (°): {K(THF)(**L**)}₂ N1-C5 1.278, C5-C6 1.426, C6-S1 1.751, S1-C9 1.761, C6-C7 1.381, C7-C8 1.391, C8-C9 1.410, C9-C10 1.407, N1-N2 7.731, C9-C10-C17 128.6, S1-C9-C17-S2 -0.1; **L**˙ N1-C5 1.266, C5-C6 1.448, C6-S1 1.731, S1-C9 1.755, C6-C7 1.376, C7-C8 1.398, C8-C9 1.398, C9-C10 1.416, N1-N2 7.483, C9-C10-C17 127.3, S1-C9-C17-S2 -13.8; Cu₂I₂(**L**˙): S-Cu 2.698, N-Cu 1.845, Cu-I 2.708, Cu1-Cu2 3.385, N1-C5 1.318, N1-N2 6.960, C9-C10-C17 125.6, S-Cu-N 80.9, N-Cu-I 132.3, Cu1-I-Cu2 77.4, I1-Cu-I2 97.5, S1-C9-C17-S2 5.5; **L**˙(BF₄)₂ N1-C5 1.258, C5-C6 1.441, C6-S1 1.729, S1-C9 1.735, C6-C7 1.381, C7-C8 1.406, C8-C9 1.383, C9-C10 1.461, C10/C17 1.392, C17-S2 1.765, S2-C20 1.708, C17-C18 1.419, C18-C19 1.381, C19-C20 1.399, C20-C21 1.459, C21-N2 1.269, C9-C10-C17 122.5, S1-C9-C17-S2 -47.6.
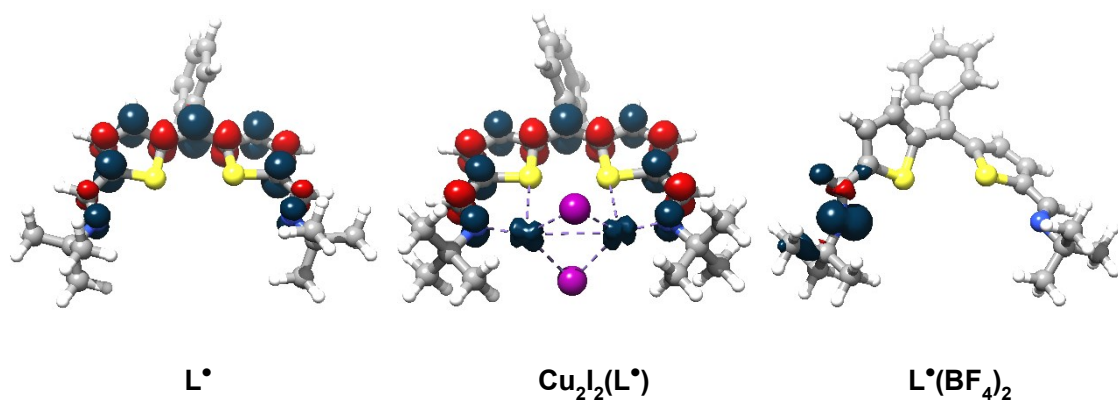
Figure S20. Spin density plot for compounds **L•**, Cu$_2$I$_2$(**L•**) and **L•**(BF$_4$)$_2$.

LUMO +1   **LUMO +2**   **LUMO +3**   **LUMO +4**

LUMO

HOMO

HOMO -1   **HOMO -2**   **HOMO -3**   **HOMO -4**
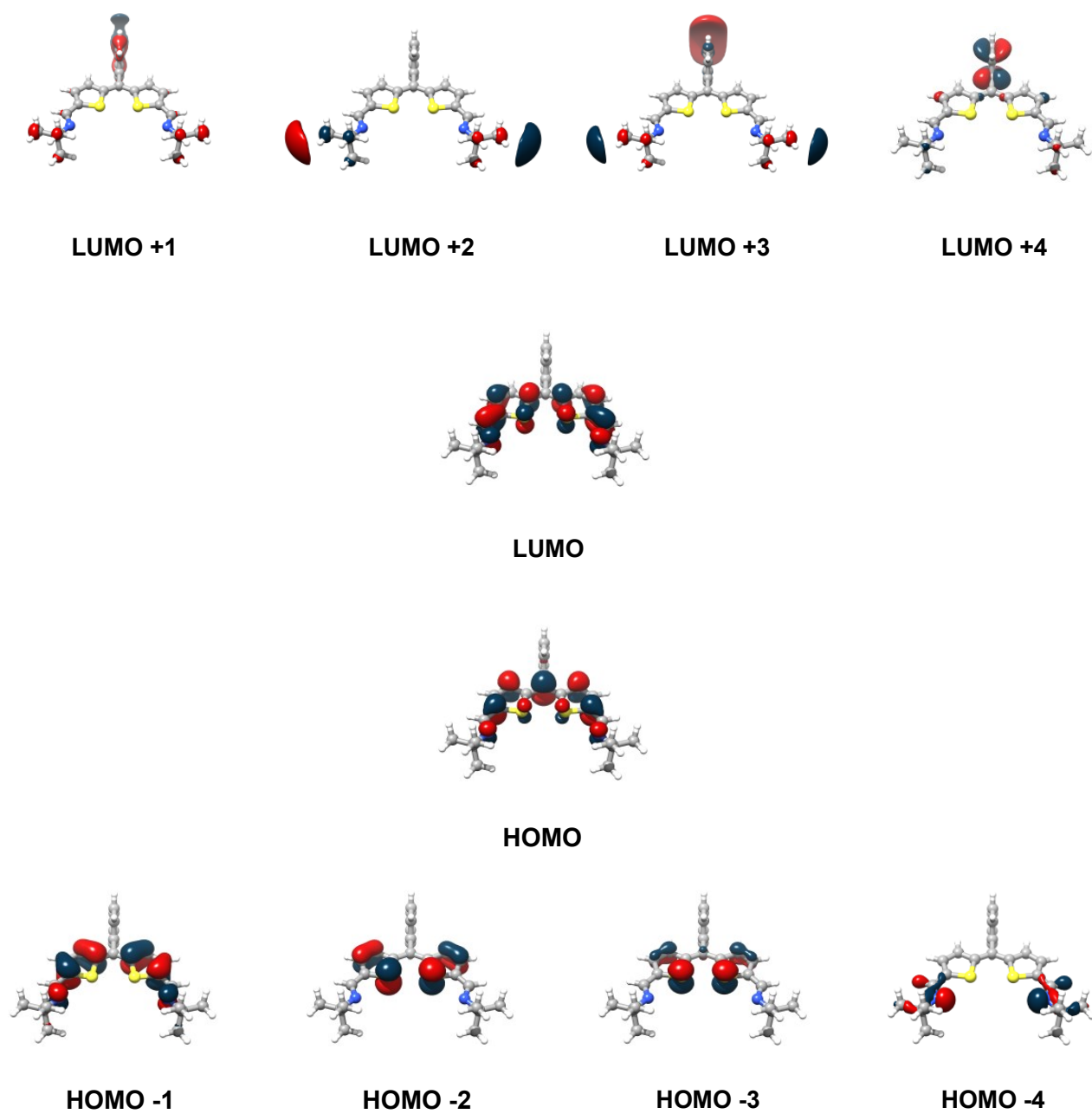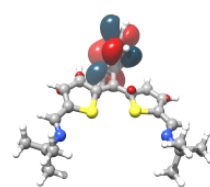
Figure S21. Molecular orbital diagram of {K(THF)(**L**)}$_2$.
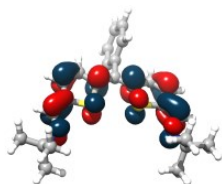
(α) LUMO +1 **(α) LUMO +2** **(α) LUMO +3** **(α) LUMO +4**

(α) LUMO

(α) SOMO
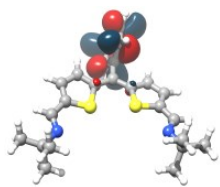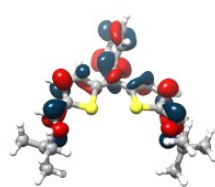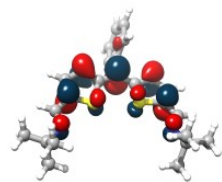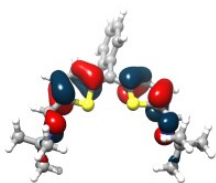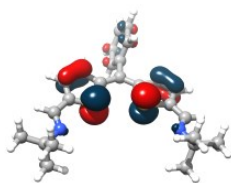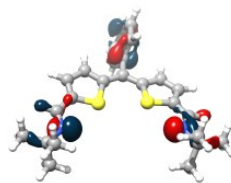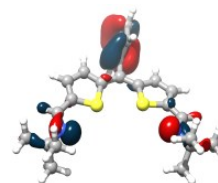
(α) SOMO -1 **(α) SOMO -2** **(α) SOMO -3** **(α) SOMO -4**

Figure S22. Molecular orbital diagram (α-configuration) of **L·**.

(β) LUMO +1 **(β) LUMO +2** **(β) LUMO +3** **(β) LUMO +4**

(β) LUMO

(β) SOMO
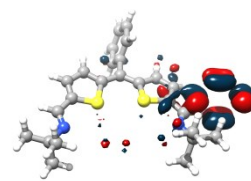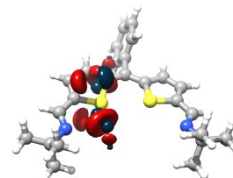
(β) SOMO -1 **(β) SOMO -2** **(β) SOMO -3** **(β) SOMO -4**

Figure S23. Molecular orbital diagram (β-configuration) of **L·**.

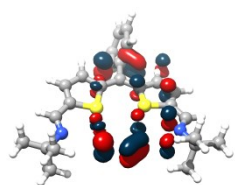(α) LUMO +1   (α) LUMO +2   (α) LUMO +3   (α) LUMO +4

(α) LUMO

(α) SOMO

(α) SOMO -1   (α) SOMO -2   (α) SOMO -3   (α) SOMO -4
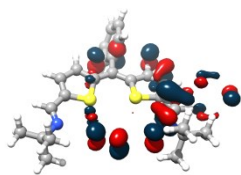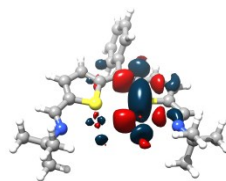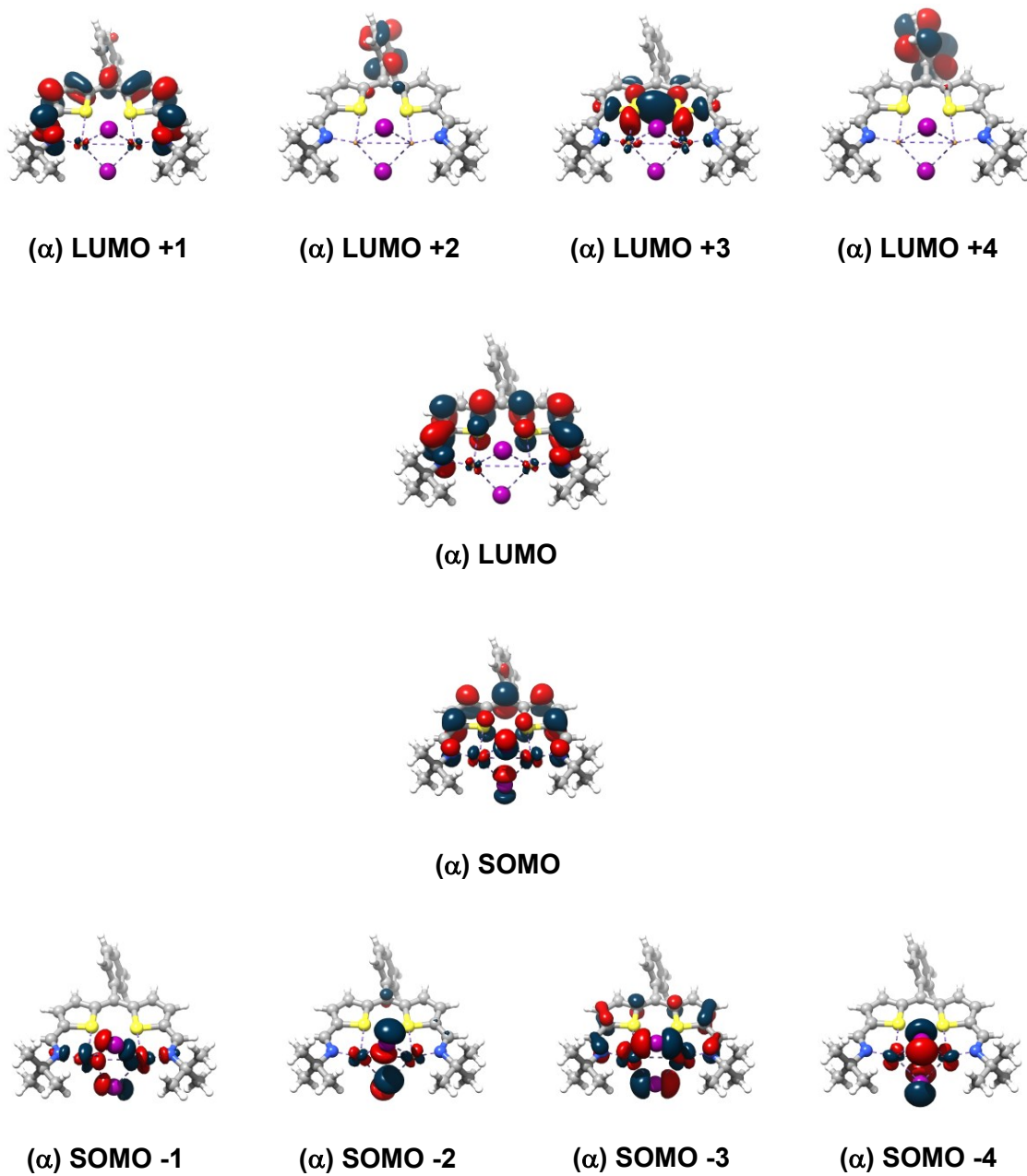
Figure S24. Molecular orbital diagram (α-configuration) of $Cu_2I_2(\mathbf{L}^{\bullet})$.

(β) LUMO +1   **(β) LUMO +2**   **(β) LUMO +3**   **(β) LUMO +4**

(β) LUMO

(β) SOMO

(β) SOMO -1   **(β) SOMO -2**   **(β) SOMO -3**   **(β) SOMO -4**
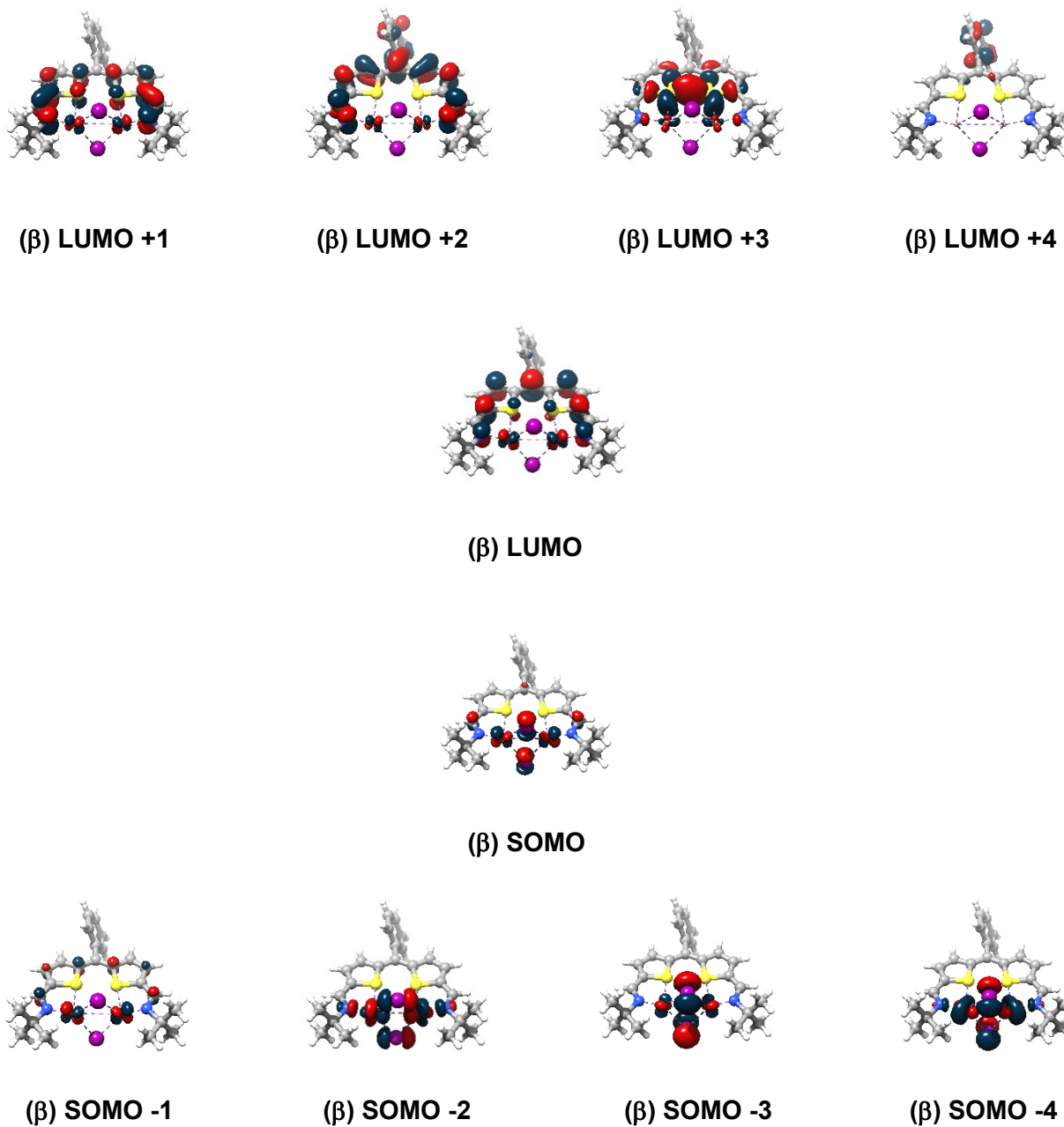
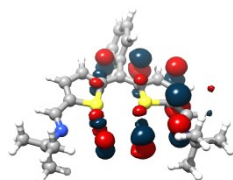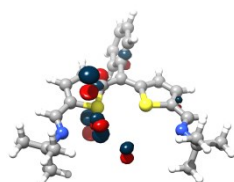**Figure S25.** Molecular orbital diagram (β-configuration) of $Cu_2I_2(\mathbf{L}^•)$.
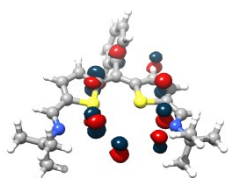
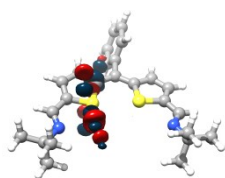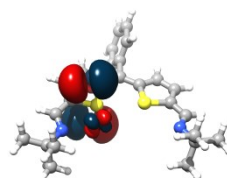(α) LUMO +1　　　(α) LUMO +2　　　(α) LUMO +3　　　(α) LUMO +4

(α) LUMO

(α) SOMO

(α) SOMO -1　　　(α) SOMO -2　　　(α) SOMO -3　　　(α) SOMO -4

Figure S26. Molecular orbital diagram (α-configuration) of **L**$^•$(BF$_4$)$_2$.

(β) LUMO +1   **(β) LUMO +2**   **(β) LUMO +3**   **(β) LUMO +4**

(β) LUMO

(β) SOMO
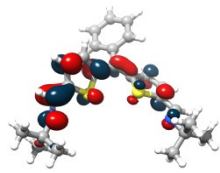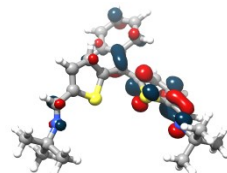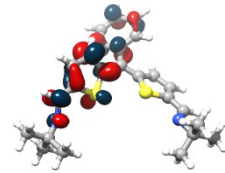
(β) SOMO -1   **(β) SOMO -2**   **(β) SOMO -3**   **(β) SOMO -4**

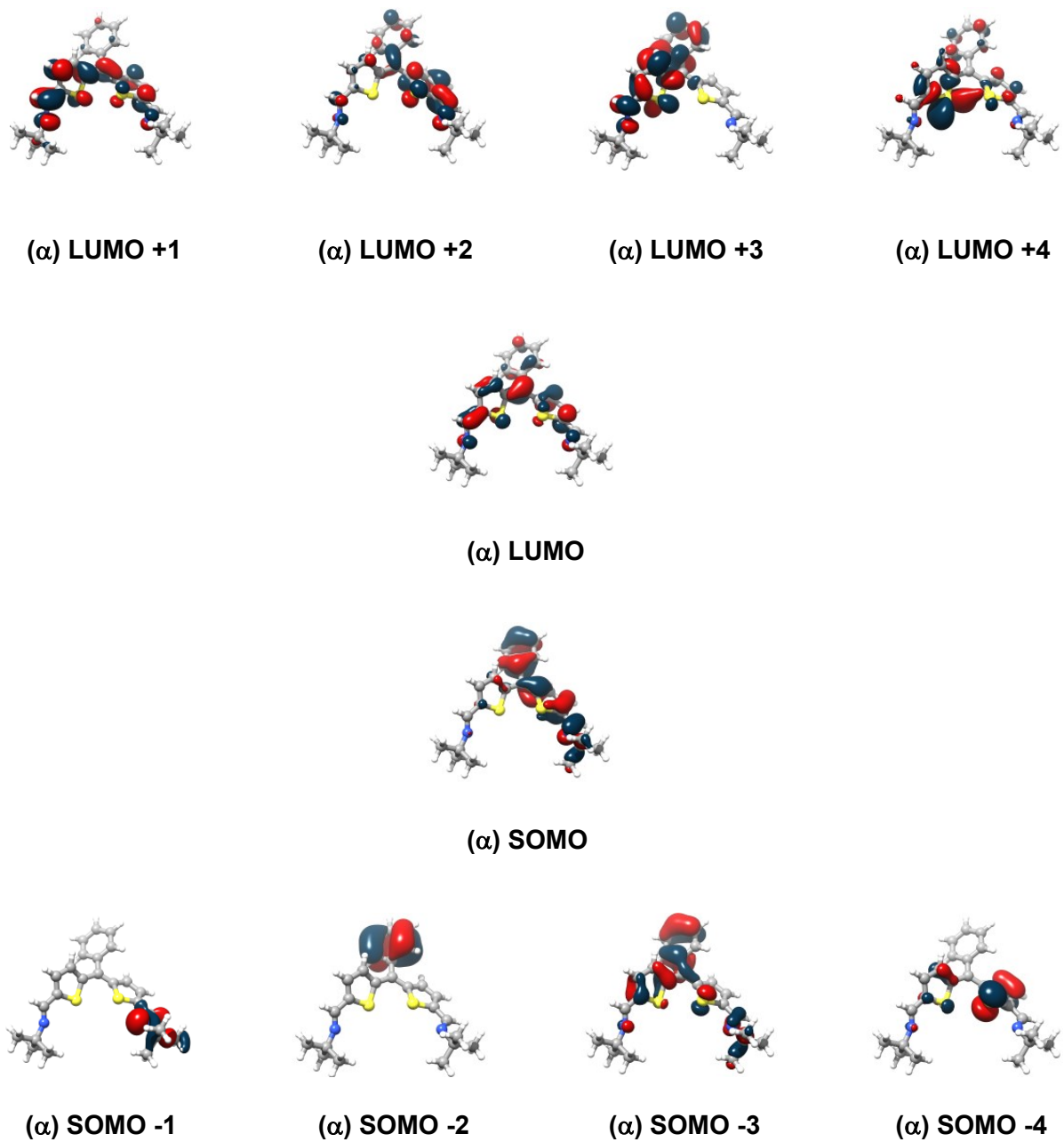**Figure S27.** Molecular orbital diagram (β-configuration) of **L·**(BF₄)₂.
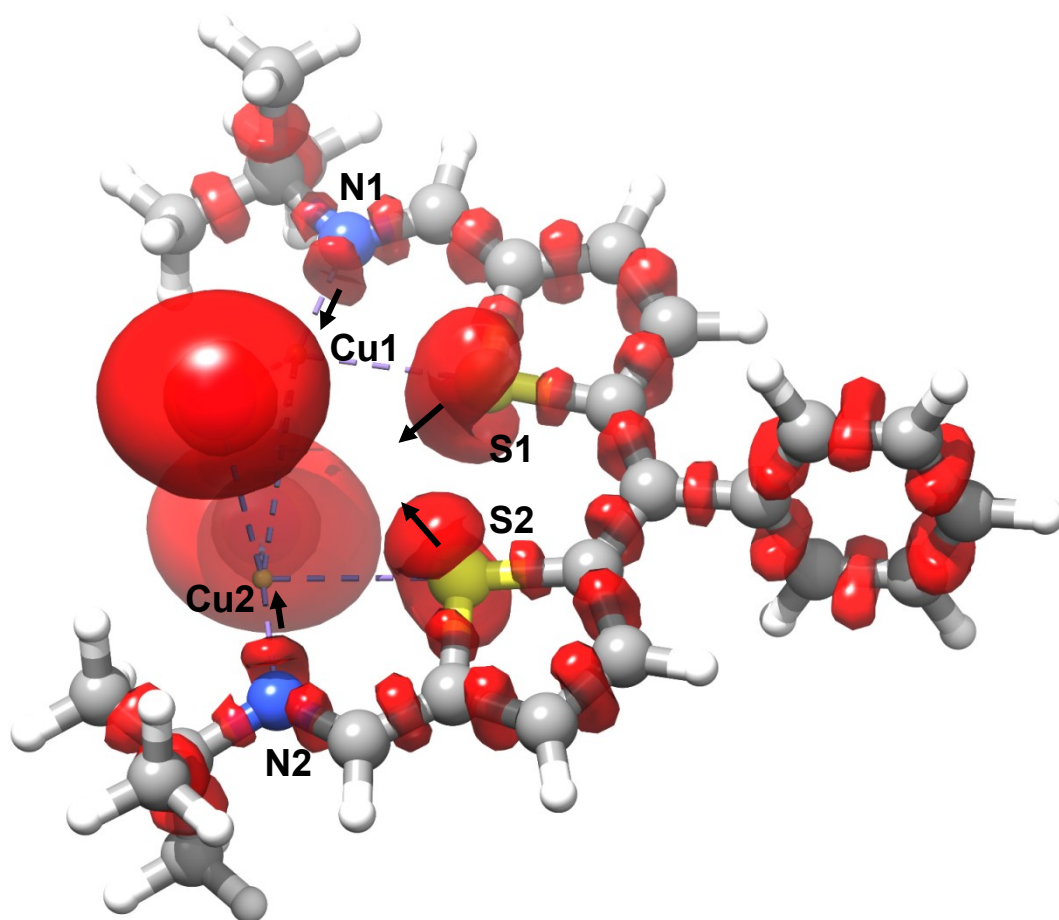
Figure S28. Electron Localization Function plot of $Cu_2I_2(\mathbf{L}^{\boldsymbol{\cdot}})$. For clarity, the calculation has been restricted to non-hydrogen atoms.

Optimized DFT Geometries

HL

Charge = 0 Multiplicity = 1

16	-2.808872	0.363305	-0.643246
16	2.458588	0.230117	-0.162956
7	5.257589	-0.824618	0.473224
7	-5.578735	-0.659654	0.148995
6	0.023365	2.159088	-0.380689
6	3.492271	-0.778323	-1.119325
6	-1.131062	-0.075313	-0.632191
6	-0.103584	0.878453	-1.194398
1	-0.438528	1.166639	-2.195545
6	-0.111849	2.155163	1.002874
1	-0.366271	1.234325	1.513710
6	1.230496	0.199108	-1.383624
6	1.616696	-0.537965	-2.463137
1	0.987693	-0.682218	-3.331608
6	-3.249295	-1.130842	0.117476
6	4.811059	-1.179073	-0.653702
1	5.368031	-1.805093	-1.358767
6	-6.974782	-0.978016	0.455107
6	-2.152044	-1.904601	0.358993
1	-2.211236	-2.877795	0.828749
6	-4.634407	-1.451575	0.424871
1	-4.777590	-2.424139	0.907027
6	0.334907	3.351064	-1.026034
1	0.443986	3.360887	-2.105142
6	2.911075	-1.098727	-2.313033
1	3.399369	-1.711910	-3.059324
6	0.070590	3.323265	1.729512
1	-0.035835	3.306691	2.807458
6	0.382727	4.508592	1.079561
1	0.520403	5.420959	1.647053
6	-0.939319	-1.301592	-0.071943
1	0.034077	-1.760996	0.023277
6	6.585810	-1.223451	0.942944
6	0.512464	4.520621	-0.302775
1	0.751206	5.442795	-0.818801
6	-7.473195	0.140692	1.375090
1	-6.942452	0.119217	2.329457
1	-8.542155	0.029134	1.571241
1	-7.299273	1.112790	0.912234
6	-7.724355	-0.919204	-0.879477

1	-7.554151	0.043314	-1.363300
1	-8.797690	-1.051177	-0.724066
1	-7.373527	-1.704591	-1.552608
6	-7.206993	-2.336357	1.119186
1	-6.870984	-3.160607	0.485314
1	-8.274317	-2.474419	1.300192
1	-6.697290	-2.409607	2.082923
6	6.363695	-1.956887	2.269070
1	5.789376	-1.330285	2.952436
1	7.319667	-2.204710	2.736263
1	5.807138	-2.882804	2.108060
6	7.353940	0.077399	1.196730
1	7.513066	0.619129	0.261788
1	8.327883	-0.132875	1.644805
1	6.787950	0.722240	1.869986
6	7.379107	-2.114707	-0.014320
1	6.863379	-3.057698	-0.211679
1	8.346266	-2.355221	0.430422
1	7.570473	-1.617690	-0.968465

{K(THF)(**L**)}₂

Charge = −1 Multiplicity = 1

16	-1.551006	-0.167450	-0.000647
16	1.550994	-0.167452	0.000987
7	-3.865411	-2.283366	-0.000067
7	3.865425	-2.283343	0.000323
6	-0.000015	2.180565	0.000033
6	-0.000024	3.674657	-0.000041
6	1.267792	1.570211	-0.000723
6	-1.267827	1.570211	0.000870
6	-3.289280	0.040982	0.001653
6	-4.205079	-1.051641	0.001657
1	-5.255593	-0.732304	0.003296
6	4.205076	-1.051614	-0.001437
1	5.255589	-0.732270	-0.003245
6	2.508539	2.240175	-0.003043
1	2.580906	3.317337	-0.004694
6	3.289269	0.041000	-0.001239
6	-2.508572	2.240166	0.003136
1	-2.580955	3.317326	0.004675
6	4.858941	-3.350457	-0.000060
6	-3.605939	1.384788	0.003474
1	-4.634208	1.729863	0.005185
6	-0.000044	6.480152	-0.000204
1	-0.000057	7.564483	-0.000266
6	0.009637	5.780089	1.199489
1	0.017184	6.317702	2.141446
6	-0.009648	4.391289	-1.195711
1	-0.017209	3.839863	-2.128731
6	3.605912	1.384810	-0.003255
1	4.634177	1.729893	-0.004942
6	-0.009718	5.779949	-1.199814
1	-0.017269	6.317453	-2.141834
6	-4.858883	-3.350520	-0.000090
6	0.009585	4.391429	1.195546
1	0.017155	3.840109	2.128627
6	4.589587	-4.199702	-1.248398
1	3.544701	-4.512820	-1.260789
1	5.229091	-5.087789	-1.270025
1	4.774159	-3.614151	-2.152136
6	6.326359	-2.904814	-0.003221
1	6.566045	-2.312476	-0.889847
1	6.976703	-3.782999	-0.003252
1	6.569199	-2.310222	0.881035

6	-6.326329	-2.904967	0.003332
1	-6.565916	-2.312788	0.890096
1	-6.976625	-3.783184	0.003294
1	-6.569349	-2.310241	-0.880786
6	-4.593971	-4.196099	-1.251866
1	-4.781912	-3.607956	-2.153224
1	-5.233442	-5.084206	-1.273736
1	-3.549102	-4.509050	-1.268953
6	4.594002	-4.196513	1.251375
1	4.781848	-3.608686	2.152962
1	5.233511	-5.084599	1.272981
1	3.549147	-4.509529	1.268290
6	-4.589422	-4.200249	1.247894
1	-3.544507	-4.513267	1.260128
1	-5.228841	-5.088406	1.269188
1	-4.774021	-3.615079	2.151875

L•

Charge = 0 Multiplicity = 2

16	-1.553729	-0.133617	-0.082950
16	1.553717	-0.133707	0.082898
7	3.740866	-2.237110	0.054574
6	0.000111	3.708240	0.000019
7	-3.740982	-2.236919	-0.054478
6	0.000057	2.217223	-0.000008
6	-1.264832	1.587998	0.102166
6	-3.577126	1.389739	0.396868
1	-4.590947	1.718537	0.584671
6	3.252862	0.070226	-0.180105
6	-2.472682	2.245948	0.354773
1	-2.528154	3.312335	0.512413
6	2.472792	2.245804	-0.354834
1	2.528331	3.312192	-0.512447
6	1.264920	1.587922	-0.102211
6	-3.252872	0.070419	0.179970
6	4.156900	-1.060795	-0.160633
1	5.206883	-0.810722	-0.343962
6	0.500152	4.415539	1.091182
1	0.889542	3.869315	1.942031
6	3.577189	1.389526	-0.396985
1	4.591018	1.718270	-0.584834
6	0.496906	5.803008	1.093269
1	0.882470	6.340681	1.951181
6	0.000222	6.500188	0.000075
1	0.000264	7.583484	0.000095
6	-0.496517	5.803091	-1.093148
1	-0.882039	6.340831	-1.951038
6	-4.156977	-1.060548	0.160501
1	-5.206976	-0.810376	0.343602
6	-0.499874	4.415623	-1.091117
1	-0.889305	3.869463	-1.941989
6	4.641580	-3.389536	0.076777
6	-4.641782	-3.389290	-0.076717
6	6.117084	-3.074959	-0.177296
1	6.273593	-2.627983	-1.162104
1	6.696513	-3.999023	-0.139813
1	6.524932	-2.399884	0.579113
6	-6.117289	-3.074591	0.177171
1	-6.273864	-2.627486	1.161910
1	-6.696771	-3.998625	0.139751
1	-6.525024	-2.399585	-0.579360

6	-4.125022	-4.351752	0.997445
1	-3.070222	-4.571075	0.828231
1	-4.688628	-5.287469	0.977232
1	-4.224620	-3.909171	1.990988
6	-4.478944	-4.027787	-1.459874
1	-5.050162	-4.956919	-1.522976
1	-3.427622	-4.246036	-1.650725
1	-4.832541	-3.350473	-2.240375
6	4.478854	-4.027959	1.459985
1	5.049971	-4.957154	1.523044
1	3.427531	-4.246074	1.650977
1	4.832634	-3.350658	2.240415
6	4.124629	-4.352025	-0.997276
1	4.224097	-3.909478	-1.990847
1	3.069847	-4.571304	-0.827900
1	4.688209	-5.287757	-0.977107

Cu₂I₂(**L•**)

Charge = 0 Multiplicity = 2

16	1.238355	-1.461370	-0.998390
16	1.238276	1.461382	0.099560
7	-1.021166	-3.424731	0.051508
7	-1.021280	3.424711	-0.051493
6	2.970309	1.254225	-0.068128
6	1.347306	-3.169055	0.137508
6	0.162224	-3.953267	0.137209
1	0.289146	-5.033621	0.204502
6	2.970355	-1.254133	0.068062
6	3.621915	0.000061	0.000010
6	3.570865	-2.508790	0.279866
1	4.637424	-2.619096	0.420057
6	-2.192640	-4.341052	-0.035049
6	0.162093	3.953282	-0.137231
1	0.288986	5.033640	-0.204504
6	2.667657	-3.567333	0.313075
1	2.951003	-4.600411	0.476537
6	-2.201643	-5.331144	1.130746
1	-1.372294	-6.041275	1.083193
1	-3.128441	-5.910023	1.115535
1	-2.145526	-4.796684	2.082630
6	5.110445	0.000079	0.000043
6	3.570763	2.508892	-0.280052
1	4.637316	2.619233	-0.420252
6	5.820522	0.621427	1.030648
1	5.273520	1.099688	1.836505
6	7.907596	0.000089	0.000113
1	8.992690	0.000094	0.000139
6	-2.192781	4.340989	0.035132
6	7.209652	0.620133	1.030893
1	7.748176	1.100994	1.841054
6	1.347189	3.169095	-0.137615
6	5.820578	-0.621274	-1.030520
1	5.273619	-1.099547	-1.836398
6	-3.433937	-3.454237	0.033239
1	-3.517808	-2.971301	1.009765
1	-4.342253	-4.036922	-0.136433
1	-3.373629	-2.680462	-0.736919
6	-2.143847	-5.057889	-1.386682
1	-2.107108	-4.328060	-2.199720
1	-3.032919	-5.679874	-1.518202
1	-1.264255	-5.702432	-1.465612

6	7.209708	-0.619966	-1.030698
1	7.748276	-1.100825	-1.840830
6	2.667520	3.567402	-0.313284
1	2.950830	4.600486	-0.476766
53	-1.974976	0.003250	2.083921
53	-1.975011	-0.003294	-2.083903
29	-1.437135	1.625776	-0.012790
29	-1.437093	-1.625811	0.012802
6	-3.434047	3.454122	-0.033038
1	-3.517983	2.971169	-1.009549
1	-4.342373	4.036769	0.136707
1	-3.373637	2.680360	0.737125
6	-2.201927	5.331064	-1.130677
1	-1.372618	6.041247	-1.083198
1	-3.128757	5.909889	-1.115406
1	-2.145851	4.796593	-2.082557
6	-2.143907	5.057849	1.386749
1	-2.107076	4.328035	2.199796
1	-3.032990	5.679805	1.518330
1	-1.264330	5.702423	1.465597

L•(BF₄)₂

Charge = 2 Multiplicity = 2

16	1.633853	-0.070322	0.212498
16	-1.631109	-0.013149	-0.244567
7	3.711476	-2.139731	0.143454
7	-3.998686	-2.115476	-0.007950
6	4.098091	-1.086899	-0.451038
1	5.079748	-0.942376	-0.908275
6	-0.027721	3.676983	-0.038975
6	0.052041	2.226189	0.011848
6	1.239696	1.571698	-0.301245
6	3.168048	0.034365	-0.531423
6	-1.151690	1.511383	0.431232
6	2.316295	2.121873	-1.043132
1	2.262154	3.098089	-1.507620
6	-3.039760	-0.040877	0.756851
6	3.386360	1.258376	-1.171791
1	4.296165	1.480220	-1.715799
6	-1.185057	4.313950	-0.533514
1	-2.014133	3.719799	-0.901318
6	-3.126415	1.069541	1.574071
1	-3.930323	1.233709	2.282402
6	-2.056678	1.959882	1.375584
1	-1.929096	2.888094	1.917363
6	-4.020834	-1.095390	0.728053
1	-4.875109	-1.000749	1.414424
6	-4.592993	-3.342666	-0.455379
6	-1.240026	5.693840	-0.610710
1	-2.118289	6.177985	-1.022584
6	1.050450	4.466361	0.412490
1	1.914647	3.990052	0.861609
6	4.573773	-3.314609	0.300091
6	-0.164407	6.462371	-0.161211
1	-0.219116	7.544786	-0.208243
6	0.973359	5.848192	0.359389
1	1.793411	6.449731	0.735019
6	4.692050	-3.531729	1.816157
1	5.224641	-2.703245	2.290622
1	5.248447	-4.451494	2.011281
1	3.703821	-3.618588	2.272906
6	-4.931897	-3.212144	-1.944290
1	-5.613767	-2.379269	-2.127508
1	-5.416922	-4.133815	-2.271302
1	-4.027503	-3.075043	-2.540132

6	5.958128	-3.184160	-0.332497
1	5.902219	-3.029374	-1.414470
1	6.517032	-4.107327	-0.167530
1	6.539863	-2.371868	0.113849
6	-5.889126	-3.487860	0.400012
1	-5.658906	-3.565285	1.464231
1	-6.359895	-4.419588	0.077729
1	-6.583724	-2.666414	0.214812
6	3.799438	-4.478777	-0.333949
1	2.806573	-4.568712	0.112504
1	4.341438	-5.412867	-0.168803
1	3.688220	-4.334569	-1.412155
6	-3.620418	-4.492887	-0.173359
1	-2.698708	-4.372909	-0.745952
1	-4.091645	-5.428109	-0.481372
1	-3.378919	-4.560931	0.889295
1	-4.091645	-5.428109	-0.481372
1	-3.378919	-4.560931	0.889295

K(THF)**L**^{N4}

Charge = −1 Multiplicity = 1

9	-2.845088	-0.040965	2.357185
9	-2.845489	0.043766	-2.355611
9	-5.527973	-0.058405	2.350489
9	-5.528382	0.026237	-2.349065
9	-6.886705	-0.024978	0.000672
7	0.680812	-1.519479	-0.002259
7	0.662649	1.564483	0.005128
7	3.216120	-3.039982	0.018141
7	3.174888	3.098973	-0.002855
6	0.799718	-2.834151	-0.022530
6	2.063846	-3.562659	-0.019790
1	1.926790	-4.655595	-0.055108
6	0.765653	2.878724	0.020859
6	-1.248187	0.011611	0.000997
6	-1.410341	-2.499400	-0.038970
1	-2.484380	-2.612133	-0.052051
6	-0.478279	-3.496900	-0.047278
6	-0.682595	1.289489	0.013549
6	-2.748576	0.002032	0.000791
6	2.023735	3.622844	0.017263
1	1.879716	4.711704	0.033917
6	-0.666025	-1.261599	-0.011895
6	-0.520937	3.527283	0.040941
1	-0.705777	4.592823	0.056483
6	-3.472348	-0.024405	1.182023
6	-1.441090	2.519755	0.035547
1	-2.516383	2.620042	0.046873
6	4.397090	-3.915574	0.007099
6	-3.472554	0.018730	-1.180481
6	4.386742	3.913184	-0.004353
6	-4.856421	-0.033461	1.194898
6	-4.856628	0.009753	-1.193434
6	-5.550974	-0.016370	0.000711
6	5.161490	3.517979	-1.266624
1	5.292305	2.435695	-1.293515
1	6.143255	4.000285	-1.289428
1	4.607377	3.811337	-2.161374
6	5.184708	3.488320	1.233605
1	4.648394	3.762168	2.145225
1	6.167663	3.968556	1.248537
1	5.313925	2.405515	1.233561
6	4.184791	5.432197	0.015416

1	3.630069	5.777248	-0.860660
1	5.157389	5.930067	0.011656
1	3.647587	5.756772	0.910018
6	5.611301	-2.992146	0.114591
1	5.613198	-2.284582	-0.716088
1	6.546536	-3.560688	0.103774
1	5.557296	-2.412702	1.037855
6	4.469177	-4.699627	-1.308475
1	3.627306	-5.388498	-1.406573
1	5.393975	-5.281313	-1.362004
1	4.442337	-4.010577	-2.155122
6	4.385109	-4.877310	1.201509
1	4.291945	-4.314539	2.132764
1	5.311553	-5.457517	1.237582
1	3.549756	-5.578309	1.144896
1	-0.650837	-4.564414	-0.067139

References

[1] G. R. Hanson, K. E. Gates, C. J. Noble, M. Griffin, A. Mitchell, S. Benson, *J. Inorg. Biochem.* **2004**, *98*, 903-916.

[2] a) G. M. Sheldrick, *Acta Crystallogr. Sect. A* **2015**, *71*, 3-8; b) G. M. Sheldrick, *Acta Crystallogr. Sect. C* **2015**, *71*, 3-8; c) G. M. Sheldrick, *Acta Crystallogr. Sect. A* **2008**, *64*, 112-122.

[3] O. V. Dolomanov, L. J. Bourhis, R. J. Gildea, J. A. K. Howard, H. Puschmann, *J. Appl. Cryst.* **2009**, *42*, 339-341.

[4] Gaussian 09, Revision E.01, M. J. Frisch, G. W. Trucks, H. B. Schlegel, G. E. Scuseria, M. A. Robb, J. R. Cheeseman, G. Scalmani, V. Barone, B. Mennucci, G. A. Petersson, H. Nakatsuji, M. Caricato, X. Li, H. P. Hratchian, A. F. Izmaylov, J. Bloino, G. Zheng, J. L. Sonnenberg, M. Hada, M. Ehara, K. Toyota, R. Fukuda, J. Hasegawa, M. Ishida, T. Nakajima, Y. Honda, O. Kitao, H. Nakai, T. Vreven, J. A. Montgomery, Jr., J. E. Peralta, F. Ogliaro, M. Bearpark, J. J. Heyd, E. Brothers, K. N. Kudin, V. N. Staroverov, R. Kobayashi, J. Normand, K. Raghavachari, A. Rendell, J. C. Burant, S. S. Iyengar, J. Tomasi, M. Cossi, N. Rega, J. M. Millam, M. Klene, J. E. Knox, J. B. Cross, V. Bakken, C. Adamo, J. Jaramillo, R. Gomperts, R. E. Stratmann, O. Yazyev, A. J. Austin, R. Cammi, C. Pomelli, J. W. Ochterski, R. L. Martin, K. Morokuma, V. G. Zakrzewski, G. A. Voth, P. Salvador, J. J. Dannenberg, S. Dapprich, A. D. Daniels, Ö. Farkas, J. B. Foresman, J. V. Ortiz, J. Cioslowski, and D. J. Fox, Gaussian, Inc., Wallingford CT, 2013.

[5] G. Igel-Mann, H. Stoll, H. Preuss, *Mol. Phys.* **1988**, *65*, 1321-1328.

[6] a) S. Noury, X. Krokidis, F. Fuster, B. Silvi, *Comput. Chem.* **1999**, *23*, 597; b) E. Matito, B. Silvi, M. Duran, M. Solà, *J. Chem. Phys.* **2006**, 125, 024301-1-024301-9; c) F. Feixas, E. Matito, M. Duran, M. Solà, B. Silvi, *J. Chem. Theory Comput.* **2010**, 2736-2742.

[7] E. F. Pettersen, T. D. Goddard, C. C. Huang, G. S. Couch, D. M. Greenblatt, E. C. Meng, T. E. Ferrin, *J. Comput. Chem.* **2004**, *25*, 1602-1612.

[8] a) K. Singh, S. Sharma, A. Sharma, *J. Mol. Catal A* **2011**, *12*, 353-356; b) O. Meth-Cohn, M. Ahmed, *J. Chem. Soc. C* **1971**, *11*, 2104-2111.

[9] J. R. Pankhurst, T. Cadenbach, D. Betz, C. Finn, J. B. Love, *Dalton Trans.* **2015**, *44*, 2066-2070.